NASA-CR-177419
19860020348

A Reproduced Copy

OF

NASA CR-177,419

Reproduced for NASA

by the

NASA Scientific and Technical Information Facility

1 Report No.	2. Government Accession No	3. Recipient's Catalog No.
NASA CR 177419		

4 Title and Subtitle	5. Report Date
Experiments on High Speed Ejectors	July 1986
	6. Performing Organization Code

7 Author(s)	8 Performing Organization Report No.
J. J. Wu	
	10. Work Unit No
	T-7527

9. Performing Organization Name and Address	11 Contract or Grant No.
J. J. Wu Sierra Madre, California 91024	Ames Research Center Purchase Order No. A40174-C
	13 Type of Report and Period Covered
	Contractor Report

12 Sponsoring Agency Name and Address	14 Sponsoring Agency Code
National Aeronautics and Space Administration Washington, D.C. 20546	505-61-71

15 Supplementary Notes

Point of Contact: Kiyoshi Aoyagi, NASA Ames Research Center, M.S. 247-2
Moffett Field, CA 94035
FTS: 464-5047 or 415-694-5047

16 Abstract

Experimental studies were conducted to investigate the flow and the performance of thrust augmenting ejectors for flight Mach numbers in the range of 0.5 to 0.8, primary air stagnation pressures up to 107 psig (738 kPa), and primary air stagnation temperatures up to 1250 deg. F (677 deg. C). The experiment verified the existence of the second solution ejector flow, where the flow after complete mixing is supersonic. Thrust augmentation in excess of 1.2 was demonstrated for both hot and cold primary jets. The experimental ejector performed better than the corresponding theoretical optimal first solution ejector, where the mixed flow is subsonic. Further studies are required to realize the full potential of the second solution ejector.

The research program was started by the Flight Dynamics Research Corporation (FDRC) to investigate the characteristic of a high speed ejector which augments thrust of a jet at high flight speeds. The program was jointly supported by the Air Force Office of Scientific Research (AFOSR) and NASA-Ames Research Center through Air Force Contract F49620-81-C-0043.

17 Key Words (Suggested by Author(s))	18 Distribution Statement
Ejector Aircraft Propulsion and Power Air-Breathing Engines	Unclassified-Unlimited STAR Category 07

19 Security Classif (of this report)	20 Security Classif (of this page)	21 No of Pages	22. Price*
Unclassified	Unclassified	80	

*For sale by the National Technical Information Service Springfield, Virginia 22161

82 pages

NASA CONTRACTOR REPORT 177419

IN-15367

Experiments on High Speed Ejectors

J. J. Wu

NASA Ames Research Center
Purchase Order Number A-40174-C
July 1986

NASA

NASA CONTRACTOR REPORT 177419

Experiments on High Speed Ejectors

J.J. Wu
Sierra Madre, California

Prepared for
Ames Research Center
under Purchase Order A-40174-C
July 1986

National Aeronautics and
Space Administration

Ames Research Center
Moffett Field California 94035

FOREWORD

The research program was started by the Flight Dynamics Research Corporation (FDRC) to investigate the characteristic of a high speed ejector which augments thrust of a jet at high flight speeds. The program was jointly supported by the Air Force Office of Scientific Research (AFOSR) and NASA-Ames Research Center through Air Force Contract F49620-81-C-0043.

With the death of the principal investigator, president, and owner of FDRC, Dr. Morton Alperin, on December 12, 1985, all effort on the program was stopped. The company, FDRC, is not doing any further research on ejectors and the existing contract was terminated. This report was prepared under the sponsorship of NASA-Ames Research Center.

I wish to express my appreciation to David Koenig, Victor Corsiglia, and Kiyoshi Aoyagi of NASA-Ames and James Wilson of AFOSR for their interest and support to this effort. I am indebted to Dr. Morton Alperin for providing his leadership during the course of this research program, and to Marilyn Stein and Trinh Nguyan for their contribution to this project. I would also like to thank Mrs. Elayne P. Alperin for her permission to use the experimental data.

Jiunn-Jenq Wu

Sierra Madre, California
June, 1986

TABLE OF CONTENTS

ABSTRACT

Experimental studies were conducted to investigate the flow and the performance of thrust augmenting ejectors for flight Mach numbers in the range of 0.5 to 0.8, primary air stagnation pressures up to 107 psig (738 kPa), and primary air stagnation temperatures up to 1250 deg. F (677 deg. C). The experiment verified the existence of the second solution ejector flow, where the flow after complete mixing is supersonic. Thrust augmentation in excess of 1.2 was demonstrated for both hot and cold primary jets. The experimental ejector performed better than the corresponding theoretical optimal first solution ejector, where the mixed flow is subsonic. Further studies are required to realize the full potential of the second solution ejector.

NOMENCLATURE

a	= primary jet area
a_*	= primary jet throat area or area at ambient exhaust
C	= discharge coefficient
D	= hydraulic diameter of the mixing duct
F	= gross thrust of the ejector, or force
L	= total length of the ejector
M	= Mach number
$\dot{m}$	= mass flow rate
n	= $(\gamma - 1)/\gamma$
P_o	= stagnation pressure
P	= pressure
R	= gas constant, or radius
r	= entrainment or mass flow ratio (= $\dot{m}_i/\dot{m}_p$)
T_o	= stagnation temperature
T	= temperature
U	= secondary or mixed flow velocity
V	= primary or injected flow velocity
X	= duct width or area
x,z	= coordinates
Z	= streamwise dimension
α	= area ratio (= X_2/a_1)
α_*	= area ratio (= X_2/a_*)
β	= orientation of primary nozzle
γ	= ratio of specific heats (C_p/C_v) = 1.4 for data presented
ΔP	= primary jet pressure rise (= $P_{op} - P_{o\infty}$)
ΔS	= total entropy production due to mixing
ΔT	= primary jet temperature rise (= $T_{op} - T_{o\infty}$)
ρ	= mass density
ϕ	= thrust augmentation

Subscripts

I	= minimum or sonic section of the secondary flow at the inlet
i	= induced or secondary flow, or inlet
m	= mixing duct
n	= inlet nose
p	= primary flow
$1,2,3$	= ejector stations
∞	= ambient or freestream conditions

LIST OF TABLES

LIST OF ILLUSTRATIONS

INTRODUCTION

A theoretical analysis of the flow through a thrust augmenting ejector by the Flight Dynamics Reasearch Corporation has been published in the AIAA Journal (References 1 and 2). That analysis evaluated the potential of the ejector as a propulsion element using the fact that the mixing of primary and secondary compresible flows in a constant area duct can result in two flow regimes (two solutions to the governing equations) after complete mixing, as described by Keenan, et al. (Reference 3). The first solution involves a subsonic flow after mixing while the second solution is characterized by a supersonic flow after mixing. References 1 and 2 also described a means for optimization of the thrust augmentation derived from ejector configurations based on both the first and second solutions. Under either solution, the investigation indicates that with proper design considerations, ejectors can be utilized to provide sufficiently large thrust augmentations to be advantageous over the entire flight spectrum of modern aircraft. The second solution at its limit point (limited by the Second Law of Thermodynamics) provides a basis for determining ejector configurations which can potentially provide much larger values of thrust augmentations than first solution configurations at all flight Mach numbers.

The theory indicates that the performance of thrust augmenting ejectors depends strongly upon the selection of the inlet and outlet configurations, where these configurations must be designed for the chosen flight and injected gas characteristics. High performing ejectors generally require high degrees of flow compression (diffusing) at their inlet, outlet or both. The compressive regions of the ejector represent the most critical elements that can be responsible for the major losses, unless their design is carefully carried out. In a conventional first solution ejector designed for operation at low subsonic speeds, the outlet generally consists of a subsonic diffuser. In the midsubsonic to transonic flight speed range, the analysis shows that the first solution ejector can achieve an acceptable performance only with the injection of high temperature, low pressure ratio gas. These gas characteristics are available only from gas generators having low thermal efficiency at the stated flight speed. Therefore , it is necessary to utilize second solution ejectors in the midsubsonic to transonic flight speed range to achieve a desireable level of ejector performance. For these ejectors, the critical element is the outlet which is generally a supersonic diffuser. Ejectors translating at supersonic speed usually have an expansion outlet for both the first and second solutions. Therefore, the major loss in an ejector translating at supersonic speeds occurs at its inlet; particularly if the design is based on a criterion with subsonic secondary flow at the start of mixing.

The theory of references 1 and 2 is predicated on first using an ideal one-dimensional compressible flow model without consideration of performance degradation due to the influence of skin friction, incomplete mixing, and wave losses in the mixing section. The inlet and outlet flows are assumed to be isentropic. Follow-on steps involve considerations of the effect of departure from the ideal model. In particular, an extensive discussion of outlet and inlet wave losses due to compression of supersonic flow has been presented in References

1 and 2. This discussion provides insight into the effect of these losses on the design of the ejector.

The purpose of this experimental study is to verify the existence of the second solution ejector flow, to observe the deviation of realistic flow from the ideal one, and to demonstrate that good ejector performance can be achieved with a properly configured ejector.

THEORETICAL CONSIDERATIONS

The performance of an ejector under either solution to the governing equations of the ejector flow problem is a function of the flight and injected gas characteristics, the cross-section of the ejector's mixing section in comparison to the total cross-section of its primary nozzles, the losses attributable to the ejector flow, and the characteristics of the secondary flow at the start of mixing. The experimental effort in the present study was conducted to simulate flight Mach number of 0.5 to 0.8. At this range of flight speeds and injection gas characteristics available from efficient propulsion system, the first solution ejectors cannot be designed to achieve a satisfactory performance, as discussed in References 1 and 2. Therefore, ejectors designed to operate in this speed range require the usage of operating principles derived from the second solution to the ejector problem, where the mixed flow is supersonic. The theoretical discussions presented here will emphasize problems associated with the second solution ejectors translating at midsubsonic to high subsonic speeds. A schematic of the theoretical ejector and some of the notation are presented as Figure 1. Additional symbols are listed in the nomenclature. A detailed theoretical analysis of the ejector problem was presented in Reference 1.

Differences between the First and the Second Solution Ejector

Figures 2-4 illustrate the distribution of thrust augmentation, experimentally observable flow parameters, and geometric requirements as a function of the Mach number (M_1) of the secondary flow at the start of mixing, for both the first and second solution to the thrust augmenting ejector problem. As shown on the figures, the optimal values of thrust augmentation for the first solution occur at values of M_1 that are slightly less than 1.0 for the flight speed and injected gas conditions specified on the figures. In general, for a second solution ejector, the distribution of thrust augmentation as a function of M_1 has two distinct points. One is a local maximum and mostly occurs at a supersonic value of M_1. The other is the highest value of thrust augmentation achievable by any ejector and occurs at a subsonic value of M_1 where the total entropy change across the mixing section (ΔS) is zero. Smaller values of M_1 represent impossible flows since the total entropy change across the mixing section is negative. Thus, this latter of the two distinct points in the distribution of the thrust augmentation as a function of M_1 for a second solution ejector is referred to as a limiting second solution - limited by the Second Law of Thermodynamics.

Significant differences between the optimal first solution ejector and the limiting second solution ejector can be observed by the examination of figures 2-4. Figures 2 and 3 represent ejectors operarting with cold primary flow. The optimal first solution ejectors require a maximum secondary to primary mass flow ratio, or a maximum secondary flow entrainment; while the limiting second solution ejectors require the minimum secondary to primary mass flow ratio allowable by the Second Law of Thermodynamics. Also indicated on figures 2 and 3, the mixing process increases the static pressure in the mixing duct for the first solution ejector, and decreases the

static pressure for the second solution ejector. The static pressure of the mixed flow for the first solution ejector has a minimum value for subsonic values of M_1; while the static pressure of the mixed flow for the second solution ejector has a maximum value. Theoretically, for subsonic values of M_1, the mixed flow static pressure cannot exist between the minimum mixed flow pressure of the first solution and the maximum mixed flow pressure of the second solution.

Figure 4 represents ejectors operating with hot primary flow. The maximum secondary to primary mass flow ratio occurs at the lower choking point, and the optimal first solution occurs at a value of M_1 slightly below that of the lower choking point. Therefore, the optimal first solution requires a near maximum secondary to primary mass ratio. Similar to the ejector operating with cold primary flow, the limiting second solution requires the minimum secondary to primary mass flow ratio allowable by the Second Law of Thermodynamics. The mixed flow static pressure varies continuously from high values for the first solution to low values for the second solution. The mixed flow static pressure at the limiting second solution represents the lowest achievable mixed flow static pressure for either solution at subsonic values of M_1.

Outlet

Under the stated conditions, figures 2 and 3 indicate that the outlets required for the first solution ejectors operating with a cold primary flow are converging subsonic nozzles for the range of M_1 that can provide a positive ejector net thrust ($\phi > 0$). At high values of M_1 (> 1), the first solution ejector may require a subsonic diffuser as an outlet, but its performance is very poor. As shown on figure 4, with the injection of hot primary gas, the first solution ejector requires a diverging subsonic diffuser with a small area ratio near its optimal performance point. In general, for the flight speeds under consideration, the first solution ejection has a maximum outlet area near its optimal performance point, and this outlet area ratio is very close to 1.0. For smaller values of α_* than that indicated on Figures 2-4, the mixed flow's total pressure may be high, so that the outlet of the first solution ejector may require a converging/diverging supersonic nozzle to achieve a supersonic exhaust flow. Since the optimal first solution ejector requires a maximum or a near maximum secondary to primary mass flow ratio, the first solution ejector must be designed to have minimum inlet blockage. If the exhaust flow is subsonic, the performance can be controlled by the appropriate selection of outlet area ratio.

The flow after complete mixing in second solution ejectors is always supersonic. Therefore, special attention must be given to the starting problem. In addition, it is essential to provide an outlet geometry capable of maintaining the supersonic flow with an efficient return to ambient pressure. As shown on Figures 2-4, the ideal (isentropic) second solution ejector outlets are either a converging or a converging/diverging (marked C/D on the figures) supersonic diffuser, similar to those shown on Figures 5b and 5c. As discussed in detail in Reference 2, these types of insentropic outlets can be replaced by nonisentropic fixed geometry outlets shown on Figures 5e, 5f, and 5g to provide a minimum outlet area capable of "swallowing"

the starting shock wave. The minimum starting area (X_s) is a function of the mixed flow Mach number ($M_2 > 1$) and the area of the mixing section (X_2) as described by the relationship,

$$\frac{X_s}{X_2} = \frac{\left(\frac{\gamma+1}{2}\right)^{\frac{\gamma+1}{2(\gamma-1)}} M_2 \left(1 + \frac{\gamma-1}{2} M_2^2\right)^{-\frac{\gamma+1}{2(\gamma-1)}}}{\left[\frac{(\gamma+1) M_2^2}{2 + (\gamma-1) M_2^2}\right]^{\frac{\gamma}{\gamma-1}} \left[\frac{\gamma+1}{2\gamma M_2^2 - (\gamma-1)}\right]^{\frac{1}{\gamma-1}}} \quad (1)$$

The converging fixed geometry outlets shown on Figures 2-4 for second solution ejectors are the type shown on Figure 5f. The area ratio of this type of outlet can be decreased after the supersonic mixed flow is established in the mixing duct to recover some of the wave losses as a result of the starting requirement. This concept of "Simple Adjustable Outlets" was discussed in Reference 2, and is shown on Figures 5h and 5i. Figure 6 indicates that significant performance degradation compared to the ideal limiting second solution ejector will occur due to wave losses associated with the fixed geometry (starting) outlets, and that the achievable thrust augmentation of the ejectors with simple adjustable outlets can recover most of the wave losses due to the starting requirement.

A simple adjustable outlet offers a feasible ejector outlet geometry for experimental study of the second solution ejectors because the outlet area ratio is the key parameter that defines the ejector outlet configuration and its associated performance. The variation of ejector outlet configurations as a function of M_1 is shown on Figures 2-4, where the solid line represents the ratio of the ejector exit area to the area of the mixing duct, and the dashed line represents the ratio of the outlet throat area to the area of the mixing duct. When the area of the ejector exit coincides with that of the outlet throat, the ejector has a converging channel as an outlet (Figure 5f), and is suitable for the application of the simple adjustable outlet. As shown on Figures 2-4, the simple adjustable outlet is applicable to the limiting second solution ejectors under the conditions specified on the figures. As indicated on Figure 3, the simple adjustable outlet is also applicable to almost the entire range of M_1 for ejectors operating at a flight Mach number of 0.81 when considering injection of cold primary air. As indicated on Figures 2 and 4, the adjustable outlet is also suitable for a limited range of M_1 for ejectors operating at a flight Mach number of 0.65 with an injection of either cold or hot primary air. Additionally, it was found that ejectors operating at a flight Mach number of 0.81 with an injection of hot primary air (similar to that indicated on Figure 4) have a limited range of M_1 where the simple adjustable outlet can be applied. Therefore, when the flight Mach number is low or the primary flow is hot and if the M_1 of a second solution ejector is not properly controlled so that a value close to that of the limiting second solution occurs, the ejector outlet may require a converging/diverging outlet instead of the simple adjustable outlet.

Inlet

As discussed earlier, the optimal first solution ejector requires a maximum secondary to primary mass flow ratio. Therefore, the inlet suitable for the first solution ejector must offer minimum blockage to the secondary flow. In contradiction, the limiting second solution ejector requires the minimum secondary to primary mass flow ratio allowable by the Second Law of Thermodynamics. Therefore, some kind of inlet blockage must be imposed to limit the secondary flow rate for a second solution ejector.

One means for achieving the desired mass flow ratio consists of the use of a sonic section (I) at the inlet, having an area ratio (X_I/X_2) which will limit the flow rate of the secondary flow (or equivalently, the Mach number (M_1) of the secondary flow at the start of mixing, as described by the theory) and produce the correct value of the secondary to primary mass flow ratio. This type of flow limiting method is similar to the "Saturated Supersonic Flow Patterns" observed by Fabri and Siestrunck in reference 4. The area ratio (X_I/X_2) can be evaluated from the theoretical value of M_1 and α, and can be shown to have the relationship,

$$\frac{X_I}{X_2} = \frac{\alpha - 1}{\alpha} M_1 \left[\frac{2}{\gamma + 1} \left(1 + \frac{\gamma - 1}{2} M_1^2 \right) \right]^{-\frac{\gamma + 1}{2(\gamma - 1)}} \qquad (2)$$

Thus, with this technique, and an adjustment for correction of X_I/X_2 for boundary layer and flow non-uniformity effects, it is possible to achieve the desired value of the Mach number (M_1) at the start of mixing and the correct mass flow ratio. This minimum secondary flow area ratio is presented at the bottom of Figures 2-4 for those special cases described on the figures.

Since section I is a sonic throat, it is conceivable that the flow after section I can be subsonic or supersonic as clearly shown on Figures 2-4. Also, Figures 2-4 show that there is a minimum value of X_I/X_2, below which the second solution flow with a subsonic value of M_1 cannot exist (shown as dashed line) due to violation of the Second Law of Thermodynamics. This minimum section of a secondary flow for a second solution ejector with subsonic value of M_1 is a function of freestream conditions, the stagnation pressure and temperature of the injected primary flow as well as of the size of the ejector (α_*), and the blockage due to the primary nozzles. Examples of the minimal area ratio of the secondary flow (X_I/X_2) needed for achievement of the limiting second solution ejector performance are presented on Figure 7 as a function of the primary flow stagnation temperature for a given primary jet stagnation pressure, freestream conditions, and for $\alpha_* = 22.65$. The values of α_* and the primary nozzle blockage are estimated from the ejector model with a 3/4" mixing section width coupled with Primary Nozzle No. 2 which will be discussed later in this document. As shown on Figure 7, the primary nozzle used in the

present experiment provides a significant blockage. If the boundary layer and flow non-uniformity effects are considered, this can prevent the achievement of the second solution flow for subsonic M_1 with low temperature primary gases. Figure 8 presents the prescribed minimum values of X_I/X_2 for second solution ejectors with subsonic M_1 as a function of the primary jet stagnation pressure for a primary jet stagnation temperature of 70 deg. F, and freestream Mach numbers of 0.65 and 0.81. Clearly, the existing primary nozzle used in the present experiment causes excessive blockage at low values of the primary jet stagnation pressure together with cold values for the primary jet stagnation temperature. The primary nozzle blockage shown on Figures 7 and 8 represents the situation when the total external cross-sectional area of the primary nozzle is placed in the mixing duct. If the primary nozzle is moved upstream in a converging inlet, this blockage can be reduced.

Effect of Temperature

By comparison of Figure 2 to Figure 4, it is evident that, at the limit point of the second solution, the thrust augmentation of the ejector injected with hot primary gas is higher than that of the ejector with cold primary gas when considering operation where other conditions remain the same. It is also evident that the thrust augmentation for the ejector injected with hot primary gas is more sensitive to the variation of M_1 than that of the ejector with cold primary gas.

For limiting second solution ejectors at a freestream Mach number of 0.65 and $\alpha_* = 25$, Figure 9 illustrates the performance of ejectors with fixed and simple adjustable outlets on a pressure/temperature map. The solid lines are iso-augmentation lines at the cruise configuration for the simple adjustable outlet while the dashed lines are iso-augmentation lines for the fixed geometry outlets. As the primary jet stagnation temperature is increased, the region of applicability for the simple adjustable outlet is significantly extended to lower primary nozzle pressure ratios. Both the fixed and the simple adjustable outlets provide excellent performance at high temperatures. There is a considerable advantage in the use of the simple adjustable outlet in its region of applicability, as shown on Figure 9.

Effect of α_*

The area ratio α_* ($= X_2/a_*$) provides a measure of the ejector's mixing duct size in relation to the throat area of the primary jet for a supercritical primary jet stagnation pressure. Figure 10 presents the ideal ejector performance as a function of α_* over the range covered in the present experimental study. As can be observed, the performance of the ideal limiting second solution ejector decreases rapidly with decreasing α_*. And at low values of α_*, the ideal performance of the limiting second solution ejector with a fixed geometry outlet is inadequate, particularly when realistic flow losses are considered. However, better observation of some basic flow phenomena associated with the second solution ejector are possible when experiments are conducted on ejectors having a low value of α_*.

TEST APPARATUS

The laboratory equipment utilized for the investigation reported in this document consists primarily of a static test rig, the associated instrumentation required for measurement of the forces, pressures, and temperatures utilized for determination of the performance of the ejector, and a schlieren system for flow visualization. In addition, a 48 position Scanivalve is used to measure pressure distribution along the ejector side walls.

The FDRC static test rig with a low pressure air system is shown on Figure 11. The basic structure consists of two components; a fixed frame assembly secured to the foundation, and a rigid assembly consisting of the low pressure air supply piping and the test model, supported by three bearing balls. This latter assembly is thus free to rotate and translate on a horizontal plane, restricted only by two flexible bellows and three load cells which provide the force and moment measurements.

The test rig has two air supply systems; a low pressure system which can continuously deliver the secondary air at stagnation pressures up to 8 psig (55 kPa), simulating a flight Mach number of about 0.8, and a high pressure system which can supply the primary air at stagnation pressures up to 110 psig (758 kPa). Compressed air of the low pressure system is supplied by a 50 HP Roots Connersville Compressor capable of delivering 1500 SCFM at 5 psig (34 kPa). Distribution of the compressed air and control of its mass flow rate and pressure is accomplished by three remotely operated valves. One valve each on two independent supply lines, and a dump valve on the by-pass line. The primary, high pressure system, ambient temperature air is supplied from a 400-gal. pressure vessel having a maximum pressure of 250 psig (1724 kPa). This compressed air is filtered and dried to a dew point of -40 deg. F (-40 deg. C). The discharge from the pressure vessel is controlled by a remote valve and pressure regulator to permit a controlled, adjustable pressure at the primary nozzle. The high pressure system is also equipped with a gas heater which is capable of heating the compressed air up to 1500 deg. F (810 deg. C). The mass flow rate in each supply line is measured with the aid of calibrated sharp edge orifices and pressure and temperature sensors.

The air storage capacity of the high pressure system permits the ejector to operate for about 1 minute with a cold primary air injection, and a longer duration with a hot primary air injection. Due to the characteristics of the gas heater in the high pressure system, it is necessary to use an auxiliary high pressure air supply to warm-up the system before the actual experiment can be conducted. This auxiliary air is supplied by a Jaeger Rotary Air Compressor, rated at 150 SCFM at 125 psig (862 kPa), which was powered by a gasoline engine.

Figure 12 shows the high pressure air supply system as it is installed on the FDRC static test rig. The gas heater for the system is visible on the left side of the photograph. Figure 13 is the general arrangement for the hot gas experiments. The ejector is in the center of the photograph. The wooden structure in the foreground is the movable schlieren system.

Pressure, temperature and force measurements by the transducers

were converted to digital signals by a Daytronic controller, and then transmitted to an IBM Personal Computer for data acquisition and processing.

MODEL DESCRIPTION

The ejector is enclosed in a box capable of maintaining the secondary air and fitted with adjustable primary nozzles. Figure 14 shows the top view and the side view of the high speed ejector assembly. In the experimental set-up, the left chamber on the side view (bottom drawing) of figure 14 is connected to the air distribution box of the FDRC static ejector rig (Figure 11). The secondary air enters this chamber from the bottom and exits to the settling chamber on the right through a 50 mesh stainless steel screen. The settling chamber and the ejector share common end walls or windows. The depth between the end walls is 3" (76.2 mm), and the width of the settling chamber is 8" (203.2 mm). As shown on Figure 14, the location and orientation of the primary nozzle can be set by using the two eccentric rings attatched to the end wall. The outlet of the ejector is remotely adjustable to provide a means for starting the second solution flow and for achieving the outlet area required for efficient operation of the second solution flow, which was discussed earlier. A photograph of the test model with plexiglas end walls (windows) is presented on Figure 15. Figure 16 is a photograph of primary nozzle No. 1, which is used in the double-array nozzle arangement shown on Figure 14.

Figure 14 describes the details of two primary nozzles used for the present experiment. Primary nozzle No. 1, which was shown on Figure 16, is a full span model. A single primary nozzle No. 1 secured to each end wall can make up an assembly of a double array of nozzles as shown on Figures 14 and 18. Primary nozzle No. 2 is a semispan model. When attached to each end wall, primary nozzles No. 2 can be used in pairs to make up an assembly consisting of an array of central nozzles as shown on Figure 19. The total exhaust area of these two primary nozzles is approximately equal, although primary nozzle No. 1 has twice the number of tubular converging nozzles than that of primary nozzle No. 2.

Figure 18 illustrates the coordinate system and dimensions defining the ejector configuration. This figure shows a fixed inlet ejector with a double array of primary nozzles (primary nozzle No. 1), but all the notations indicated on the figure can be applied to the adjustable inlet ejector with an array of central nozzles shown on Figure 19. For a fixed inlet ejector, the nose radius (R_n)is 0.15" (3.81 mm), and the inlet radius (R_1) is 2" (50.8 mm), and the total inlet length (Z_1) is 0.75" (19.05 mm). For fixed inlet ejectors, the location of the center of the inlet nose is 0.25" (6.35 mm) away from the ejector's mixing duct side wall ($(X_n-X_2)/2 = 0.25$"). The width of the constant area mixing duct (X_2) varies from 0.25" (6.35 mm) to 1.0" (25.4 mm). When $X_2 = 1.0$" (25.4 mm), the total ejector length (L) can vary from 3.1" (78.74 mm) to 4.6" (116.84 mm). Dimensions for other ejectors investigated are presented on Table I. The hydraulic diameter (D) of the mixing duct is calculated from the relation (Reference 5),

$$D = \frac{4 \times \text{cross-sectional area}}{\text{wetted perimeter}} \qquad (3)$$

to indicate the relative potential for frictional losses when

comparing ejectors of the same total length. For low frictional losses, small values of length-to-diameter are desired.

The hot gas ejector shown on Figure 19 has an adjustable inlet and an array of central nozzles. The nose radius (R_n) of the inlet is identical to that of the fixed inlet ejectors, but the total inlet length (Z_i) is slightly longer than that of the fixed inlet ejectors. With a proper adjustment of X_n or z_p, the inlet can provide a minimum cross-section to limit the secondary mass flow rate, and produce the desired value of the secondary-to-primary mass flow ratio, as discussed earlier.

All ejector models are provided with pressure taps on both side walls at an interval of approximately 0.25" (6.35 mm) for measurement of wall pressure distributions.

The converging inlet with double array of primary nozzles shown on Figure 18 is similar to that used in an investigation of a jet-diffuser ejector described in Reference 6. Reference 6 correlated experimental results with the two-dimensional potential flow theory to provide a set of empirical rules for setting the primary nozzle attitude to achieve the best first solution ejector performance. Typical results of the application of this empirical rule to the fixed inlet configurations shown on Table I are presented on Table II. The ideal setting of the adjustable inlet with an array of central nozzles shown on Figure 19 is that $\beta_p = 0$. The variation of β_p shown on Table II is due to the usage of a single eccentric ring for the attachment of the primary nozzle No. 2 to the ejector's end wall.

DATA REDUCTION

The expeirmental set-up permitted three independent observations of the ejector flow and performance. Wall pressures were measured by a Scanivalve on both side walls. A schlieren system was utilized for flow visualization. Generally, the ejector flowfield can be evaluated by comparing the wall pressure distribution to the schlieren photograph. The load cell readings were utilized in conjunction with mass flow, pressure, and temperature measurements in the primary and secondary flow systems to determine the thrust augmentation achieved under each ejector configuration.

The performance of a thrust augmenting ejector is evaluated by comparisca of the net thrust of the ejector to the net isentropic thrust of its primary jet when discharging to ambient pressure. This ratio, called thrust augmentation, can be expressed as,

$$\phi = \frac{F - (\dot{m}_s + \dot{m}_p)\, U_\infty}{\dot{m}_p\, (V_{p\infty} - U_\infty)} \tag{4}$$

for an "air breathing" gas generator, when both the ejector and its gas generator are operating at the same freestream conditions. In Eq. (4), the quantity F is the gross thrust of the ejector, $\dot{m}_s U_\infty$ is the ram drag of the secondary flow, $\dot{m}_p U_\infty$ is the ram drag of the primary flow, and $\dot{m}_p V_{p\infty}$ is the gross isentropic thrust of the primary jet. It is evident that accurate measurements of the ejector's gross thrust, the primary and secondary mass flow rates and stagnation conditions are required to determine the ejector performance. The velocity terms in Eq. (4) can be calculated from the stagnation conditions of the corresponding flow as follows,

$$U \text{ or } V = \sqrt{\frac{2}{n} R\, T_o \left[1 - \left(\frac{P_\infty}{P_o}\right)^n\right]} \tag{5}$$

Table III utilizes ideal limiting second solution ejectors with fixed geometry outlets to illustrate the order of magnitude of various parameters involved in the determination of ejector performance at a sea level condition of 14.7 psia and 70 deg. F. The ejector geometry and flow characteristics described on Table III are similar to that of the actual experiments performed on the hot gas ejector shown on Figure 19.

It is clear that the ram drags constitute the major portion of the ejector's gross thrust. Accurate assessment of the gross thrust and the ram drags is essential for evaluating the ejector performance. Extensive efforts were made to assure the accuracy of these force measurements. Appendices A, and B present a version of the result of calibration of the FDRC test rig used for the data reduction in the later part of this experimental program.

The calibration of the test rig was performed in three steps; 1)basic calibration, 2) static test, and 3) dynamic test. The basic calibration was performed to obtain the characteristics of the transducers and the test rig under various loads. Pressure transducers were pressurized within their appropriate pressure range to obtain correlation factors between the reading and the applied pressure. The scanning speed of the Scanivalve was determined to assure reliable readings. The load cells were calibrated individually using certified weights before installation on the test rig. The calibration of the test rig was performed by pulling the rig at various locations and directions with various weights, so that the force and moment can be evaluated from the load cell readings.

The static test was performed by pressurization of various air supply ducts, individually or in combination, of the test rig within the range of pressure encountered in the experiment. As shown previously on Figure 11, the low pressure air system has three major parts; the stationary duct, the floating Leg #1, and the floating Leg #2. The stationary duct is connected to the compressor by a flexible bellows, and is connected to the floating Leg #1 and the floating Leg #2 of the test rig by two flexible bellows. Since these flexible bellows transmit axial loads, the connecting structures will experience a pressure force when the bellows are pressurized. The tare forces due to the pressurization of the low pressure air supply system were obtained by applying pressure to 1) the stationary duct, 2) the combination of the stationary duct and the floating Leg #1, 3) the combination of the stationary duct and the floating Leg #2, and the entire low pressure system. The ducting arrangement of the high pressure air supply system, as shown on Figure 12, also pressurized to obtain the tare forces. The results of these efforts are summarized in Appendix A.

To provide an overall calibration of the entire test rig and the associated instrumentation, the dynamic test was performed on the low pressure and the high pressure air supply systems. Tests on the low pressure air supply system were performed on various ejector models with primary nozzles removed and the end walls sealed. Air was supplied by Leg #1 only, Leg #2 only, and both Legs #1 and #2. Meaurements included pressures, temperatures, and load cell readings. In addition, the pressure distribution on the ejector's side wall was measured so that the duct loss in the ejector could be estimated. As mentioned earlier, the low pressure air supply system had three major components, and each component had its own characteristic pressure. The characteristic pressures on each component were determined from the fact that at a given stagnation condition of the air supply, the ejector (used as a nozzle) has an identical thrust when air is supplied by Leg #1, Leg #2, or both legs. The ejector chosen for this evaluation was the 1" ejector and the stagnation conditions of the air supply were 5 psig and 140 deg. F.

In order to evaluate the mass flow rate of the air supply, it is neccesary that the stagnation conditions of the exhaust flow are known. The total temperature of the exhaust flow is identical to that of the measured plenum temperature in view of the energy conservation law. The total pressure of the exhaust flow can be evaluated by using the conservation laws of mass flow and energy, and the pressure distribution along the sidewall of the ejector (nozzle). It can be

shown that for a compressible flow in a constant area duct, the governing equation is,

$$\frac{P_2}{P_1} = \frac{M_1}{M_2}\sqrt{\frac{2 + (\gamma - 1)\, M_1^2}{2 + (\gamma - 1)\, M_2^2}} \tag{6}$$

Eq. (6) can be utilized to calculate the total pressure loss if the static pressure loss for the subsonic flow is known, or,

$$\frac{P_{o2}}{P_2} = \left(\frac{1 + \sqrt{1 + K}}{2}\right)^{1/n} \tag{7}$$

where,

$$K = 4\left(\frac{P_1}{P_2}\right)^2 \left[\left(\frac{P_{o1}}{P_1}\right)^{2n} - \left(\frac{P_{o1}}{P_1}\right)^{n}\right] \tag{8}$$

With the calculated stagnation pressure and the measured stagnation temperature, the exhaust velocity (U) can be obtained by using Eq (5). And the mass flow rate ($\dot{m}$) can be evaluated from the measured thrust (F),

$$\dot{m} = F / U \tag{9}$$

In general, the mass flow rate calculated from Eq. (9) corresponds well with that derived from the stagnation conditions of the exhaust flow and the geometric setting of the ejector (or nozzle). The mass flow rates were correlated to the Reynolds number of the orifices to obtain calibration curves for both Leg #1 and Leg #2 of the low pressure air supply system when the system pressure was relatively low (< 5 psig). For higher pressures and temperatures, corrections were neccesary to provide accurate mass flow rates for different ejector models at different test conditions. The details are presented in Appendix B.

The dynamic test for the high pressure system was conducted similarly, except that the exhaust total pressure was measured by a pitot tube. The exhaust total pressure was correlated to the test rig pressure measured near the entrance of the primary nozzle. Generally, the nozzle exhaust total pressure (in absolute unit) was about 96% of

the pressure measured on the test rig for both the primary nozzle No. 1 and the primary nozzle No. 2. The primary nozzles used for the present experiment were converging supersonic nozzles, therefore, the relation between the thrust and mass flow rate differed from that shown on Eq. (9). The mass flow rate and the thrust of the primary nozzle can be expressed as (Reference 7),

$$\dot{m}_p = \sqrt{\frac{\gamma}{R}} \left(\frac{2}{\gamma + 1}\right)^{\frac{\gamma + 1}{2(\gamma - 1)}} \frac{P_{op}}{\sqrt{T_{op}}} A_* \tag{10}$$

$$F_p = \left[2 \left(\frac{2}{\gamma + 1}\right)^{\frac{1}{\gamma - 1}} P_{op} - P_\infty\right] A_* \tag{11}$$

where A_* is the effective total exhaust area of the primary nozzles. Since the orifice flow meter installed in the high pressure air supply system was of the standard ASME type, the calibration effort only resulted in a minor correction to the orifice equations given in Reference 8.

Instead of relying on a orifice flow meter for measuring the primary mass flow rate, Eqs. (10) and (11) can be correlated to the expirement by the introduction of the discharge coefficient (C) and known coefficient of thermal expansion for the 300-series stainless steel (about 0.00001/deg. F) used for the model construction,

$$A_* = a_*[1 + 0.00001(T_* - 530)]^2 C \tag{12}$$

where,

$$T_* = \frac{2}{\gamma + 1} T_{op} \qquad (\text{in } ^\circ R)$$

and, a_* is the total nozzle area at room temperature. Correlation of the discharge coefficient (C) to the Reynolds number at the entrance of the primary nozzle shown on figure 17 (d = 0.469" at room temperature) provides a means for evaluating the primary mass flow rate for given primary jet stagnation conditions. The results are presented on Figures 20 and 21. This approach was used in the later part of this experimental program, and provided a better quality of experimental data, since less instrumentation was utilized.

RESULTS AND DISCUSSIONS

Initially, the ejector experiments were conducted using fixed inlet ejectors (Table I) with injection of cold primary flows. The primary purpose of these tests was to investigate the existence of the second solution ejector flows. Ejector performances were also measured to determine the basic design requirements for various components of the ejector, such as the length of the mixing duct (Z_m) and the simple adjustable outlet. Upon the installation of the heater, it was necessary to provide an adjustable inlet for optimization of the ejector performance, as discussed in "Theoretical Considerations." Unfortunately, the hot gas experiments were ended under an unusual circumstance, as described in the "Foreword" of this document. However, some valuable information was aquired as a result of this limited investigation. All tests were conducted by initially starting the secondary flow and adjusting its pressure to simulate the desired flight Mach number (M_∞), and later increasing the primary flow pressure level to the desired value. The wall pressure distributions are presented as the averages of the pressures on both side walls, i.e., pressures at corresponding points on each side wall are averaged.

Evidence of the Second Solution Flow

Figure 22 illustrates pressure distributions on a quarter-inch ejector model having an outlet area ratio of 1.01 and whose other characteristics are described on the figure. The value of α_* indicated on the figure was calculated from the area of the mixing section and the experimentally measured primary mass flow rate. This ejector was tested over a range of primary plenum pressures from P_{op}/P_∞ = 2.86 to 8.76, at sea level. The corresponding schlieren photographs for higher pressures are shown on Figure 23. Although none of the pressures reached the value corresponding to a sonic expansion of the secondary flow from its stagnation condition, as shown on Figure 22, a normal shock wave started to appear in the mixing section at a primary pressure ratio of 4.90 (Figure 23a). As the primary pressure ratio increased, the normal shock wave moved downstream. When the primary pressure ratio reached 6.25, the normal shock wave reached the exit section of the ejector (Figure 23c). As the primary pressure ratio increased further, oblique shock waves appeared at the exit of the ejector, as shown on Figures 23d-23g. Since the pressure in the mixing duct was not sufficiently low for the secondary flow to form a sonic throat (Figure 22), the observed supersonic flow must have a stagnation pressure higher than that of the unmixed secondary flow. This could only be achieved as a result of mixing of the primary and secondary fluids. The fact that the mixed flow achieved a supersonic speed is clear evidence of the existence of the second solution to the ejector flow problem.

The maximum ideal first solution outlet area ratios of this ejector with subsonic values of M_1, as determined from the analysis of References 1, are shown on Figure 24. The observation during the above described experiments indicates that supersonic flow after mixing can be achieved throughout the ejector's mixing duct for primary nozzle pressure ratios greater than 6.25, where the maximum ideal first

solution outlet area ratio is 0.905, as shown on Figure 24. Since the ejector outlet area ratio was 1.01, the second solution flow throughout the mixing duct was established when the outlet area ratio was about 12% larger than the maximum isentropic outlet area ratio of the first solution.

Figure 25 describes the theoretical limits on the mixed flow static pressure. As discussed earlier, for subsonic values of M_1, the mixed flow static pressure cannot exist between the minimum mixed flow pressure of the first solution and the maximum mixed flow pressure of the second solution. A comparison of Figures 22 and 25 indicates that the curve with the lowest primary pressure ratio ($P_{op}/P_\infty = 2.86$) can be identified as the first solution flow; while the other curves cannot satisfied this theoretical limitation. This deviation from the theory is probably due to the effect of boundary layer, and/or departures of the flowfield from the ideal one-dimensional flow assumption used in the theory.

The experimental measurements of the secondary-to-primary mass flow ratios are presented on Figure 26. The maximum mass flow ratio prescribed by the theory is also presented for comparison. It is clear that the actual mass flow ratio is only slightly less than that of the theoretical maximum value. The ejector performance of this series of tests is generally very low, as indicated on Figure 27. Other tests conducted at higher freestream Mach numbers achieved thrust augmentations of about 0.8. The low performance of this ejector is probably due to: 1) low performance associated with small α_*, as shown on Figure 10; 2) excessive ejector length, as indicated on Table I, where $L/D > 7$; and 3) an ejector configuration that was not properly optimized.

To further illustrate the fact that the mixing process can result in a supersonic mixed flow with much larger mass flow ratios, tests were performed with a fixed value of $P_{op}/P_\infty = 5.83$ at a freestream Mach number of 0.81 while varying the outlet area ratio over the range from 0.9 to 1.3. The maximum ideal outlet area ratio for these conditions with subsonic values of , as given by the theory, is 0.981 for first solution ejectors (subsonic mixed flow). The corresponding ideal maximum mass flow ratio is 7.1. Results shown on Figure 28 and observations on the schlieren screen indicate the presence of shock waves in the diverging outlets for outlet area ratios greater than 1.05. A typical schlieren picture taken when the outlet area ratio was 1.1 is presented as Figure 29. Wave patterns due to supersonic primary flows are shown near the inlet of the ejector (left side of the picture), and a near normal shock wave in the diverging outlet (right side of the picture) is evidence of a supersonic mixed flow. Figure 28 also shows that for outlet area ratios greater than 1.05, the wall pressure decreases as mixing proceeds. This is in agreement with the theoretical expectations for second solution flows as discussed earlier.

Performance of Ejector with Fixed Converging Inlet

Due to instrumentation system problems, the ejector performance measured during the series of tests that resulted in the wall pressure distribution of Figure 28 for the one-inch ejector was not reliable. Limited tests were conducted later to evaluate the performance of this

ejector. Typical results, shown on Figure 30, indicate that the ejector performance can achieve a level equal to or greater than that of the ideal optimal first solution ejector when the outlet area ratio is about 1.05. Limited attempts were made to reduce the outlet wave losses by reducing the outlet area ratio after supersonic mixed flow was established. This resulted in a collapse of the supersonic flowfield established inside the ejector duct.

Since the ejector can establish a supersonic flow throughout the mixing duct only when the outlet area ratio is greater than 1.0, as discussed earlier and shown on Figure 28, and the application of a simple adjustable outlet requires a supersonic mixed flow at an outlet area ratio less than 1.0, the concept of the simple adjustable outlet could not be successfully applied. Instead, an extension plate which can provide small angles relative to the outlet side wall was installed on the ejector to establish a converging/diverging geometry for the outlet. The total ejector length (L) was 5.6" and the ratio of the total ejector length to the hydraulic diameter of the mixing duct (L/D) became 3.73 after this modification.

Typical ejector performance is presented on Figure 31, and the wall pressure distribution and the measured ejector's duct width are shown on Figure 32. A comparison of the ejector performance of Figure 31 and the pressure distribution of Figure 32 indicates that at a low freestream Mach number of 0.647, the ejector performance is low and the pressure in the mixing duct increases as the mixing proceeds. This is characteristic of the first solution ejector. As the freestream Mach number increases, the ejector performance increases, and the shock wave activity appears near z/X_2 of about 2 and the mixed fluid is discharged as a subsonic flow.

Since the supersonic mixed flow was compressed to a subsonic flow inside the ejector to provide good ejector performance exceeding that of the ideal optimal first solution ejector, this ejector behaves like a second solution ejector with a converging/diverging fixed geometry outlet as described in Reference 2. The theoretical limits of the mixed flow static pressure for subsonic values of M_1 are shown on Figure 33. A comparison of Figures 32 and 33 indicates that the wall pressures inside the ejector are below the minimum mixed flow static pressure of the first solution, and above the maximum mixed flow static pressure of the second solution. In other words, realistic flows can exist between these two theoretical flows derived under the assumption of a one-dimensional compressible fluid. This is further supported by the fact that the ejector performance varies gradually, instead of a sudden jump, from low performance similar to that of the first solution ejector at low freestream Mach numbers to high performance similar to that of the second solution ejector at high freestream Mach numbers, as shown on Figure 31.

Exploratory Tests of Hot Gas Ejector

The unique feature of the hot gas ejector (Figure 19) is that it provides an adjustable inlet so that the secondary flow rate can be controlled to achieve the desired value required by second solution ejectors. An adjustable outlet is also provided to accomplish an efficient discharge of the mixed flow to ambient pressure. Generally, tests were conducted with the injection of hot as well as cold primary

flows for a given ejector inlet and outlet setting. Although the gas heater in the primary air supply system is capable of heating the primary flow to a temperature of 1500 deg. F (816 deg. C), most of the hot gas tests was performed at a primary gas stagnation temperature of 1250 deg. F (677 deg. C) to avoid possible overheating of the stainless steel heat exchange coil.

The wall pressure distributions of this ejector under different test conditions are shown on Figures 34-38. Schlieren photographs are presented on Figures 39 and 40, and typical ejector performances are described on Figures 41-46.

Figures 34-36 are the wall pressure distributions for the ejector injected with a cold primary flow at a stagnation pressure of about 107 psig (734 kPa) with various inlet and outlet settings. The pressure at which the secondary flow reaches a sonic speed ($M_1 = 1$) is also shown on the figures. Theoretically, for subsonic values of M_1, the minimum mixed flow pressure (P_2/P_∞) of the first solution is 1.283, and the maximum mixed flow pressure of the second solution is 0.634, at the primary and the secondary flow conditions stated on the figures. The minimal area (X_I/X_2) of the secondary flow for second solution ejectors with subsonic values of M_1, estimated by using Eq. (2), is 0.793.

As indicated on Figure 34, when the ejector inlet setting parameter (X_n - see Figure 18) is greater than or equal to 1.006" ($X_I/X_2 = 0.80$ as calculated from the ejector dimensions specified in Table I and the dimensions of the primary nozzle No. 2 shown on Figure 17), the secondary flow had a static pressure representing a subsonic flow speed near the exit of the primary nozzle. This suggests a subsonic value of M_1. When X_n is less than or equal to 0.974" ($X_I/X_2 = 0.76$), the static pressure on the ejector's inlet wall was below that of a sonic secondary secondary flow ($M_1 = 1$), and this low pressure was maintained well into the mixing duct ($z > 0$), indicating a possible supersonic value of M_1. As shown on Figures 35 and 36, with an increase of the outlet area ratio, the region of the supersonic flow extended downstream in the ejector duct while the inlet flow remained practically unchanged. Therefore, the minimal area ratio (X_I/X_2) of the secondary flow for second solution ejectors with subsonic values of M_1 derived from the theory provides a good agreement with the experimental results for the cold gas tests. Also shown on Figures 34-36 is that, except for $X_I/X_2 = 0.8$ and $X_n = 1.006$" (Figure 36), the mixed flow pressures (P_2/P_∞) are below the minimum mixed flow pressure of the first solution, and are near or below the maximum mixed flow pressure of the second solution when the mixed flow is supersonic.

The schlieren photograph for $X_n = 1.124$" at a freestream Mach number of 0.8 is shown on the bottom picture of Figure 39. Since the center part of the photograph was overexposed, only two of the four diamond shape wave patterns observed on the schlieren screen are shown on the picture.

Typical ejector performances of the above described experiments are shown on Figure 41. These results indicate that the ejector can achieve good performances, higher than that of the ideal optimal first solution ejector, if the Mach number (M_1) of the secondary flow at the start of mixing is subsonic ($X_n \geq 1.006$", or $X_I/X_2 \geq 0.80$). This is consistent with the theoretical conclusion discussed earlier. The best

ejector performance occurs near an outlet area ratio of about 0.9, a value close to that of the limiting second solution with a fixed geometry outlet. However, at this outlet area ratio, the wall pressure distribution (Figure 36) is below the minimum mixed flow pressure of the first solution, and is above the maximum mixed flow pressure of the second solution. A theoretical calculation similar to that shown on Figure 3 for the flow conditions stated on Figure 36 indicates that, at the outlet area ratio of 0.9, the ideal first solution has a mixed flow pressure (P_2/P_∞) of 1.37. Although the wall pressure distribution at the outlet area ratio of 0.9, shown on Figure 36, behaves more like the first solution flow (increasing pressure as the mixing is proceeding), the maximum mixed flow pressure is well below that of the ideal first solution.

Other performances of the ejector with the injection of cold primary flow, at a lower primary jet stagnation pressure of 77 psig (531 kPa), are shown on Figures 43 and 45, for a converging inlet with X_n = 1.236". Figure 45 represents the ejector configuration when the primary nozzle discharge point was moved further inside the mixing duct (z_p = 0.065"). The wall pressure distributions are shown on Figure 37. In general, these cold gas experiments conducted at a lower primary stagnation pressure exhibit a behavior similar to that obtained for higher primary stagnation pressures as discussed previously.

Typical schlieren photographs for the cold gas tests are presented on Figure 39 for various freestream Mach numbers. The primary nozzle discharge point appears on the left edge of the pictures. The top picture is for a freestream Mach number of 0.65, where a normal shock is visible on the second diamond shape wave pattern. As the freestream Mach number increases, the diamond shape pattern widens and increases in number so that the supersonic flow region is extended further downstream. As discussed earlier, the bottom picture shows only two diamond patterns, instead of the four observed on the schlieren screen during the test. This is due to overexposure in the center part of the picture. The schlieren photographs of the hot gas tests are presented on Figure 40. Generally, the wave patterns are similar to that of the cold gas tests with a higher primary flow stagnation pressure as shown on Figure 39. The top picture of Figure 40, where the freestream Mach number is 0.65, represents a situation where the supersonic flow is not fully developed, and the general appearance of the wall pressure distribution is similar to that of Figure 37 at an outlet area ratio (X_3/X_2) of 0.95 or 0.90.

The hot gas tests were conducted at a primary flow stagnation pressure of 75 psig (517 kPa) and a primary flow stagnation temperature of 1250 deg. F (677 deg. C) for various inlet and outlet configurations. Figure 38 presents the typical wall pressure distributions for various inlet settings with an outlet area ratio of 1.1, where the flow in the mixing duct is supersonic, at a freestream Mach number of 0.8 and α_1 of 23.3. The minimal area (X_I/X_2) of the secondary flow for second solution ejectors with subsonic values of M_1 is 0.741. The minimum mixed flow pressure (P_2/P_∞) of the first solution is 0.913, and the maximum mixed flow pressure of the second solution solution is 0.866, for subsonic values of M_1.

Examination of the pressure distributions on the inlet wall ($z < 0$), reveals that subsonic secondary flow can exist only when X_n

is greater than or equal to 1.044" (X_I/X_2 = 0.85). This experimental minimal area (X_I/X_2) of the secondary flow for second solution ejectors with subsonic values of M_1 is considerably larger than the theoretical value of 0.741. The details of this deviation from the theory are unknown. But this deviation suggests that the heated primary nozzles has a significant effect on the secondary flow in the inlet of the ejector.

Typical ejector performances of the hot gas tests are shown on Figures 42, 44, and 46. Generally, the ejector injected with hot primary gas has the same level of performance as the ejector injected with cold primary gas. It is evident from the examination of Figures 41-46 that the best performance of the ejector injected with hot primary gas seems to occur at an outlet area ratio close to 1.0, a value higher than that for the best performing ejector injected with cold primary gas. Therefore, the theoretical advantage of achieving a high ejector performance with hot gas injection at a small outlet area ratio was not realized in the present experimental set-up.

It was observed during this series of testing of the hot gas ejector (Figure 19) that the ejector performances are low when the static pressures near the inlet nose of the ejector are very low compared to the pressure of a sonic secondary flow. Therefore, the local supersonic flow near the inlet nose may have contributed wave losses to the secondary flow that degraded the ejector performance. Improvement in the ejector inlet design can probably improve the ejector performance.

CONCLUSIONS AND REMARKS

Experimental studies were conducted to investigate the flow and the performance of thrust augmenting ejectors for flight Mach numbers in the range of 0.5 to 0.8, primary air stagnation pressures up to 107 psig (738 kPa), and primary air stagnation temperatures up to 1250 deg. F (677 deg. C). The area of the ejector's mixing duct varies from 7.55 to 30.2 times that of the minimum area of the primary jet.

Generally, the second solution flow (supersonic flow after mixing) was established throughout the constant area mixing duct when the ejector had an outlet area ratio greater than the maximum outlet area ratio of the first solution (subsonic mixed flow) with a subsonic secondary flow at the start of mixing.

The concept of the simple adjustable outlet, which reduces wave losses by decreasing the outlet area ratio after the supersonic flow is established in the mixing duct, could not be applied successfully to the one-inch ejector with a fixed converging inlet. However, the one-inch ejector achieved thrust augmentations of about 1.2 to 1.3, which is better than the optimal performance of the first solution ejector, for flight Mach numbers in the range of 0.75 to 0.81. A converging/diverging fixed geometry outlet was installed for these tests.

At an inlet setting that provided subsonic secondary flow near the primary nozzle exit, the hot gas ejector had a low performance when the outlet area ratio was large and the mixed flow was supersonic (second solution flow). This was caused by excessive wave losses for the supersonic mixed flow as it returns to the ambient pressure through the oversized outlet. The ejector generally gave its best performance at an outlet area ratio where both the first and the second solution flows can exist. Thrust augmentation in excess of 1.2 was demonstrated for both hot and cold primary flows.

The adjustable inlet provided for the hot gas ejector was effective in controlling the secondary flow rate. But, when trying to adjust condition to reach sonic flow at the minimum cross-section of the inlet, it appears that local supersonic flow occured near the inlet nose and this might have created undesirable inlet losses. This phenomenon requires further investigation to minimize the inlet loss and improve the ejector performance.

This experimental study verified the existence of the second solution ejector flow, and demonstrated that a properly configured ejector can achieve better performance than that of the ideal optimal first solution ejector. However, the theoretical advantages of hot gas injection and the concept of the simple adjustable outlet could not be demonstrated for the initial test configurations and limited test conditions. To achieve optimal performance, ejector geometries must be tailored to flow conditions. This requires systematic investigations of test configuration over a wide range of flow conditions. These investigations are warranted by the promising results of the initial test effort presented in this report.

REFERENCES

1. Alperin, M. and Wu, J. J., "Thrust Augmenting Ejectors, Part I," AIAA J., Vol. 21, No. 10, October 1983, pp. 1428-1436.

2. Alperin, M. and Wu, J. J., "Thrust Augmenting Ejectors, Part II," AIAA J., Vol. 21, No. 12, December 1983, pp. 1698-1706.

3. Keenan, J. H., Neumann, E. P., and Lustwerk, F., "An Investigation of Ejector Design by Analysis and experiment," Journal of Applied Mechanics, Vol. 17, No. 3, 1950, pp. 299-309.

4. Fabri, J. and Siestrunck, R., "Supersonic Air Ejectors," Advances in Applied Mechanics, Vol. 5, Academic Press, New York, 1958, pp. 1-34.

5. Schlichting, H., "Boundary-Layer Theory," McGraw-Hill Book Co., N. Y., 1968, pp. 575.

6. Alperin, M. and Wu, J. J., "Recent Development of a Jet-Diffuser Ejector," Journal of Aircrait, Vol. 18, December 1981, pp. 1011-1018.

7. Shapiro, A. H., "The Dynamics and Thermodynamics of Compressible Fluid Flow," Vol. I, The Ronald Press Co., N.Y., 1953, pp. 100-103.

8. Bean, H. S. (Ed.), "Fluid Meters, Their Theory and Application," 6 Ed., The American Society of Mechanical Engineers, N. Y., 1971.

Table I Ejector Dimensions

X_2	R_n	X_n	R_i	Z_i	Z_m	L	D	L/D
1.00	0.15	1.50	2.00	0.75	1.5-3.0	3.1-4.6	1.500	2.07-3.07
0.75	0.15	vary	vary	1.00	2.400	4.500	1.200	3.750
0.50	0.15	1.00	2.00	0.75	2.000	3.8C8	0.857	4.443
0.25	0.15	0.75	2.00	0.75	1.675	3.250	0.462	7.042

Notes: i) all dimensions in inches.
ii) D = hydraulic diameter of the mixing duct.

Table II Typical Primary Nozzle Attitude

X_2	z_p	x_p	β_p (deg.)	Remarks
1.00	-0.463	0.350	8.0	
0.75	-0.13 to 0.13	0.000	-0.4 to 0.4	adjustable inlet (Fig. 19)
0.50	-C.565	0.209	10.0	
0.25	-C.558	0.128	10.0	

Table III. Typical Parameters for Evaluation of Thrust Augmentation

Primary Total Pressure, psig	77.0	77.0	75.0	75.0
Secondary Total Pressure, psig	6.0	7.6	6.0	7.6
Primary Total Temperature, F	70.0	70.0	1250.0	1250.0
Freestream Total Temperature, F	124.5	137.0	124.5	137.0
Alpha-Star	22.0	22.0	23.3	23.3
Mass Flow Ratio (see Note)	3.895	4.188	6.693	7.260
Thrust Augmentation (see Note)	1.418	1.436	1.627	1.648
Primary Mass Flow, slugs/sec	.00668	.00668	.00343	.00343
Secondary Mass Flow, slugs/sec	.02602	.02798	.02299	.02494
Primary Jet Velocity, ft/sec	1610.27	1610.27	2879.06	2879.06
Freestream Velocity, ft/sec	808.78	897.21	808.78	897.21
Primary Gross Thrust, lbf	10.756	10.756	9.889	9.889
Primary Jet Ram Drag, lbf	5.402	5.993	2.778	3.082
Primary Jet Net Thrust, lbf	5.354	4.763	7.111	6.807
Secondary Flow Ram Drag, lbf	21.043	25.099	18.593	22.373
Ejector Gross Thrust, lbf	34.037	37.932	32.940	36.673
Ejector Net Thrust, lbf	7.592	6.840	11.569	11.218

Note: ideal limiting second solution with fixed geometry outlet

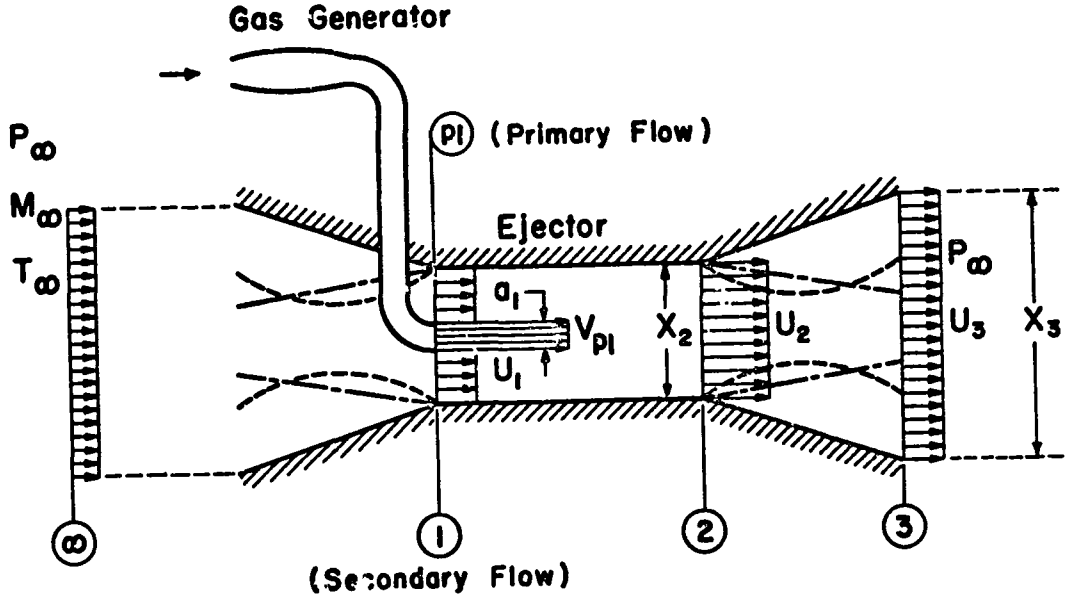

Figure 1. Schematic representation of ejector

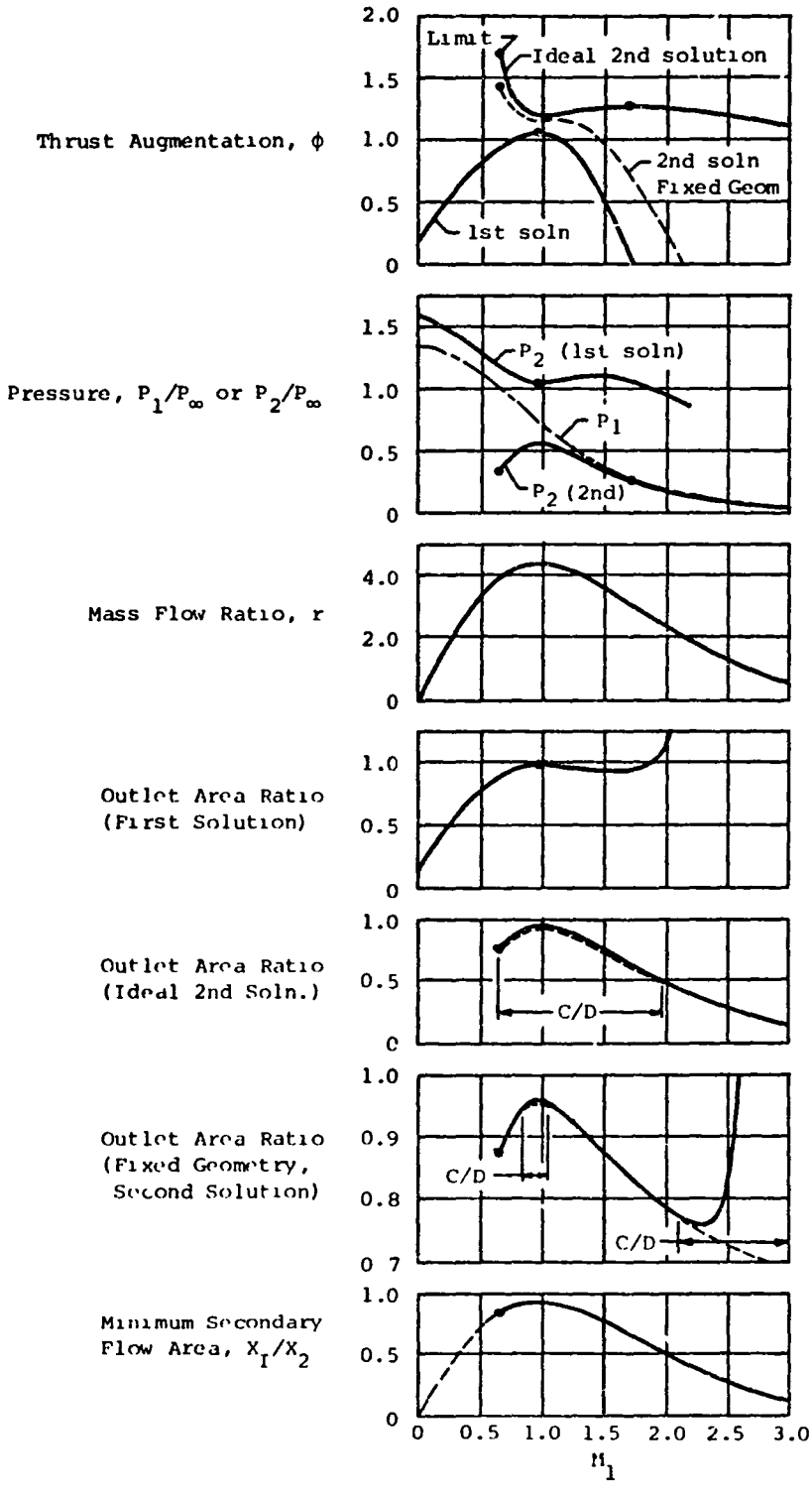

Figure 2 Ejector characteristics with cold primary flow, $M_\infty = 0.65$, $\alpha_* = 22.65$, $T_{op}/T_\infty = 1$, $P_{op}/P_\infty = 6.1$

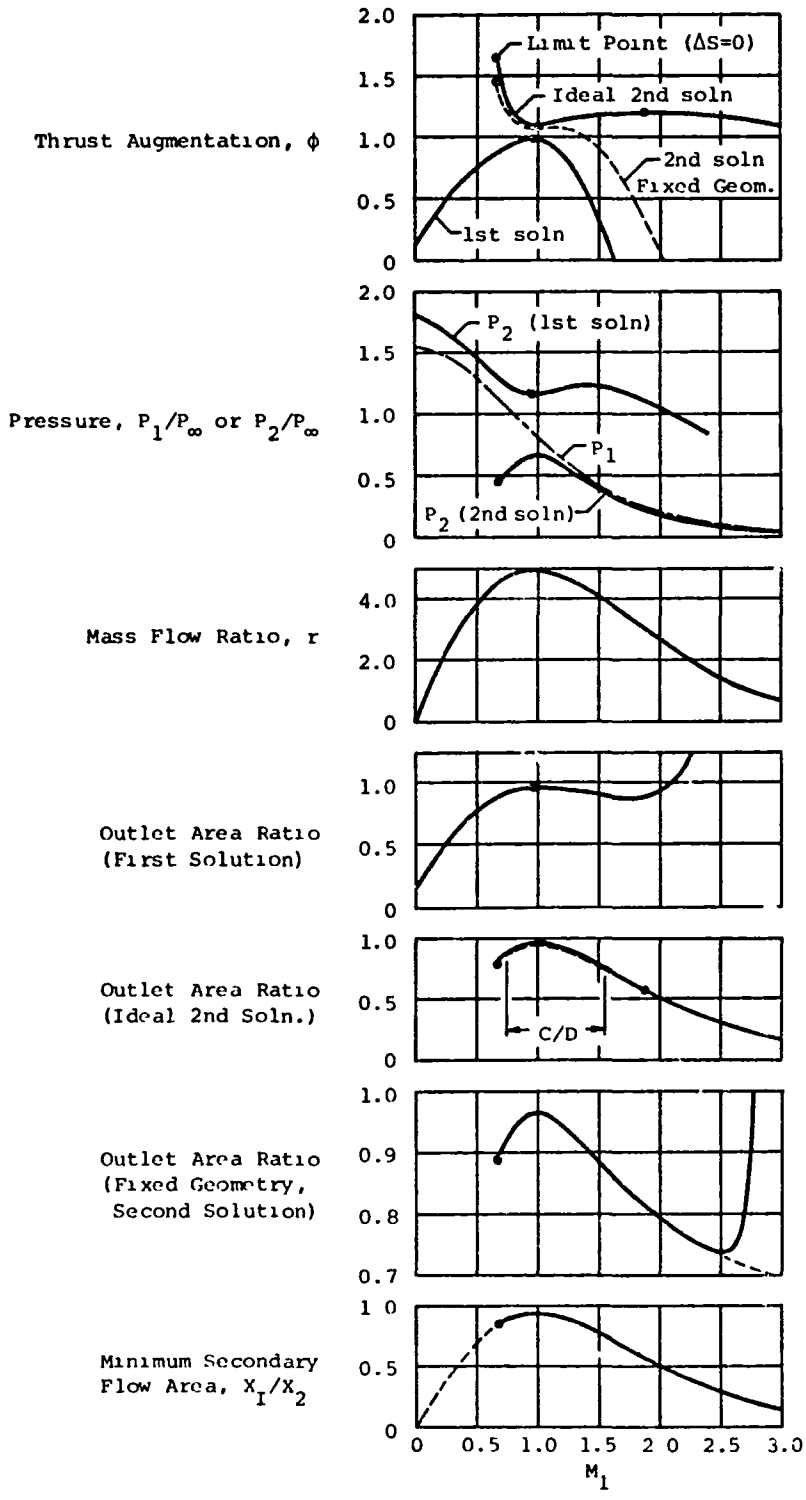

Figure 3. Ejector characteristics with cold primary flow, $M_\infty = 0.81$, $\alpha_* = 22.65$, $T_{op}/T_\infty = 1$, $P_{op}/P_\infty = 6.1$

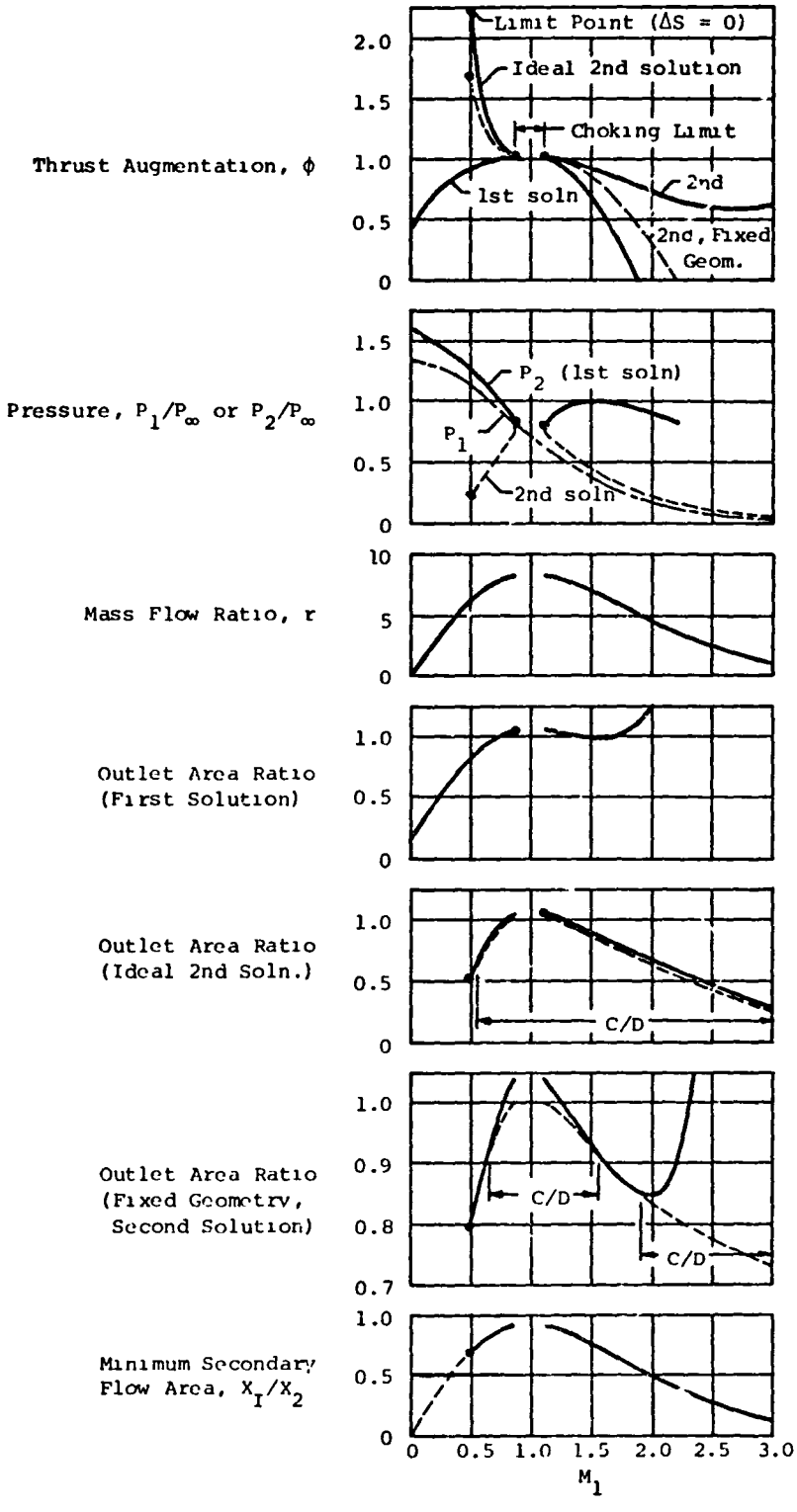

Figure 4. Ejector characteristics with hot primary flow, $M_\infty = 0.65$, $\alpha_* = 22.65$, $T_{op}/T_\infty = 3.7$, $P_{op}/P_\infty = 6.1$

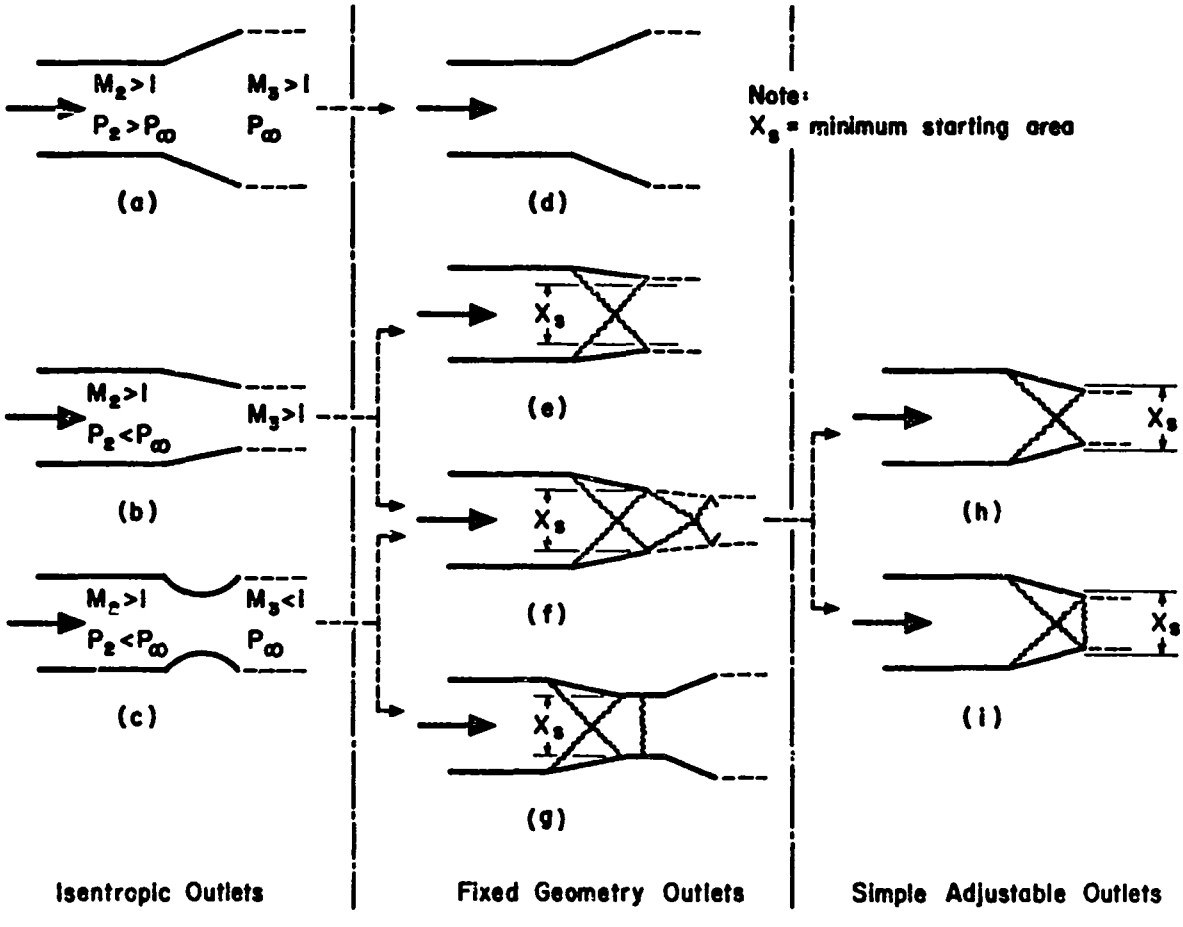

Figure 5. Schematic outlets for second solution ejectors

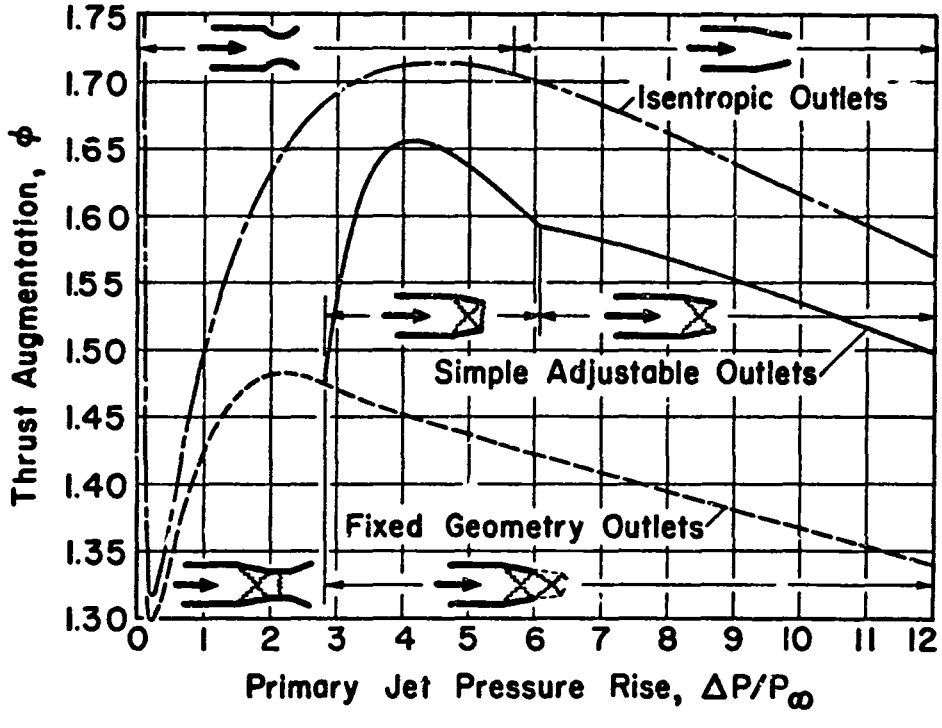

Figure 6. Influence of outlet wave losses on performance of limiting second solution ejectors, $M_\infty = 0.65$, $\alpha_* = 25$, $T_{op} = T_\infty$

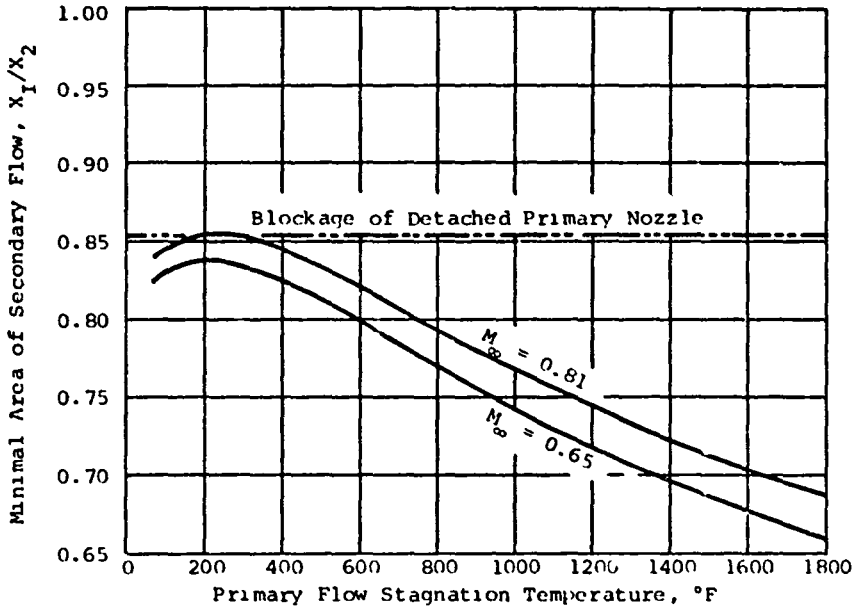

Figure 7. Influence of primary jet temperature on minimal area ratio of the secondary flow for second solution ejectors with subsonic M_1, $\alpha_* = 22.65$, $P_{op} = 75$ psig, $P_\infty = 14.7$ psia, $T_\infty = 70$ °F

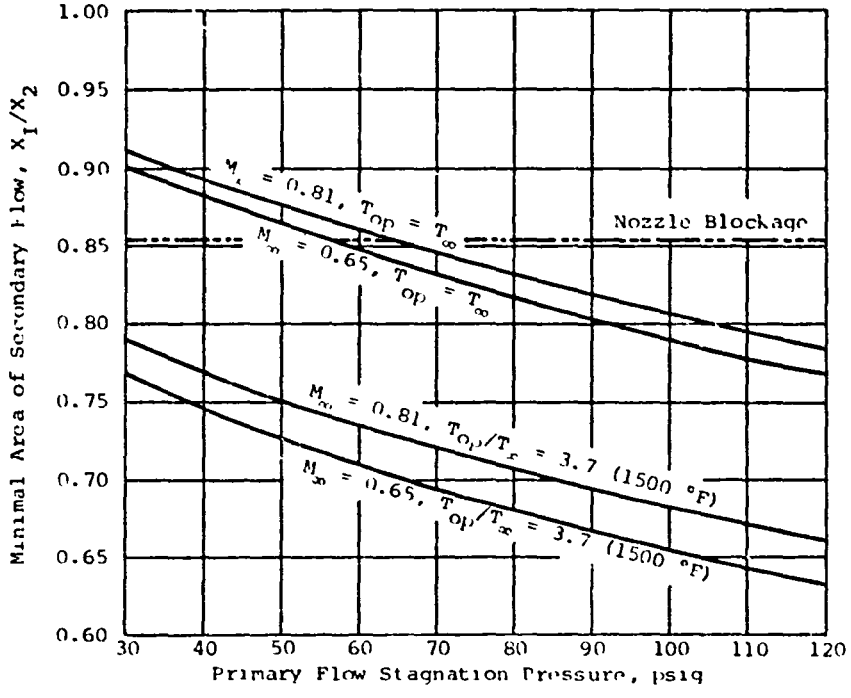

Figure 8. Influence of primary jet pressure on minimal area ratio of the secondary flow for second solution ejectors with subsonic M_1, $\alpha_* = 22.65$, $P_\infty = 14.7$ psia, $T_\infty = 70$ °F

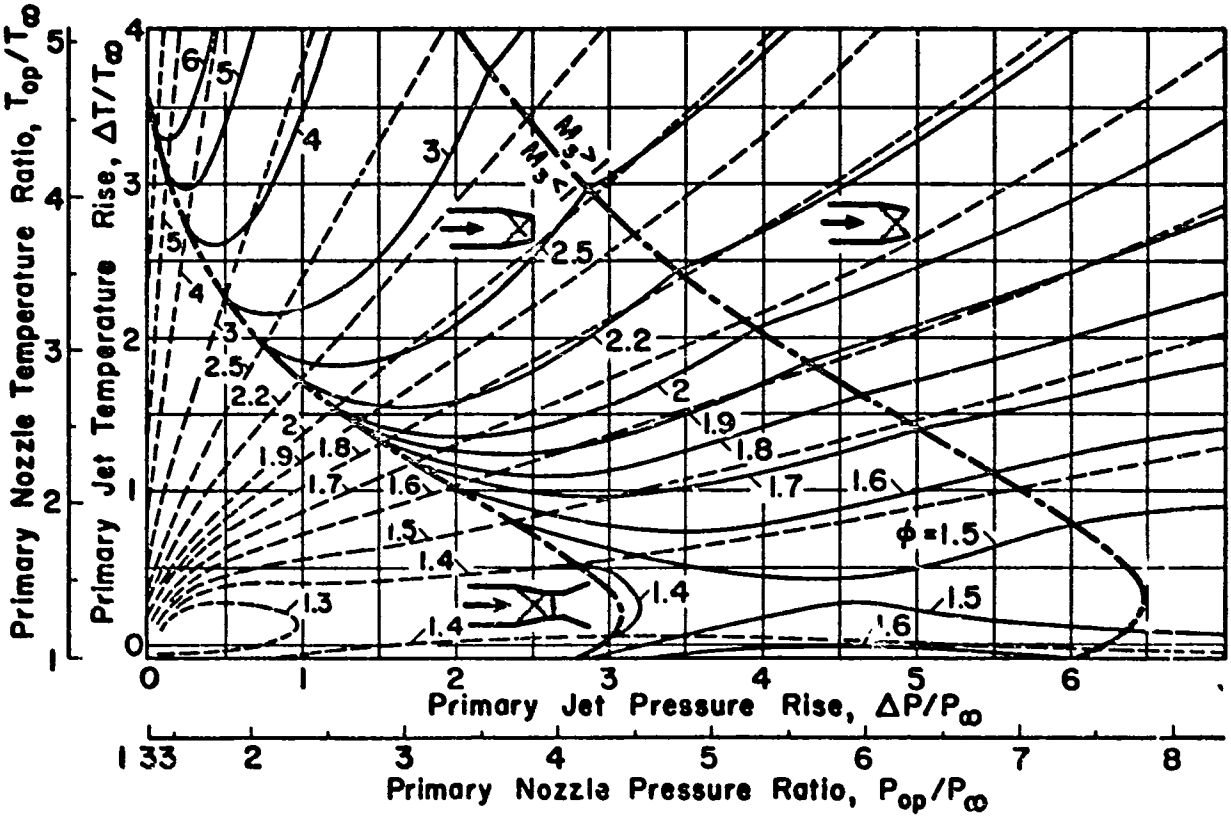

Figure 9. Performance of limiting second solution ejectors with outlet wave losses, $\alpha_* = 25$, $M_\infty = 0.65$

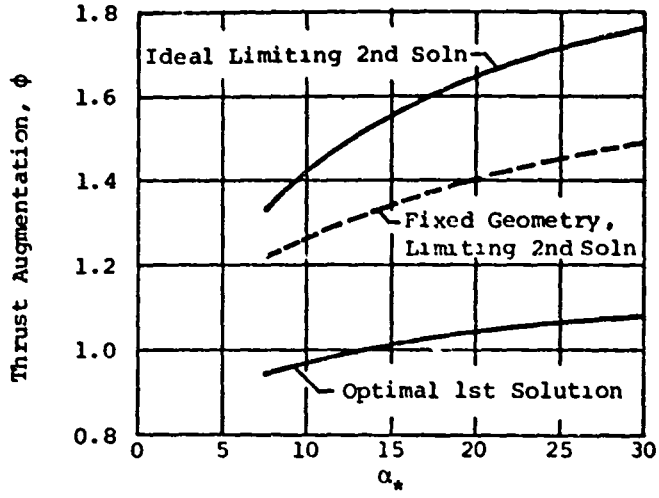

Figure 10. Influence of α_* on ejector performance, $M_\infty = 0.65$, $P_{op}/P_\infty = 6.1$, $T_{op}/T_\infty = 1$

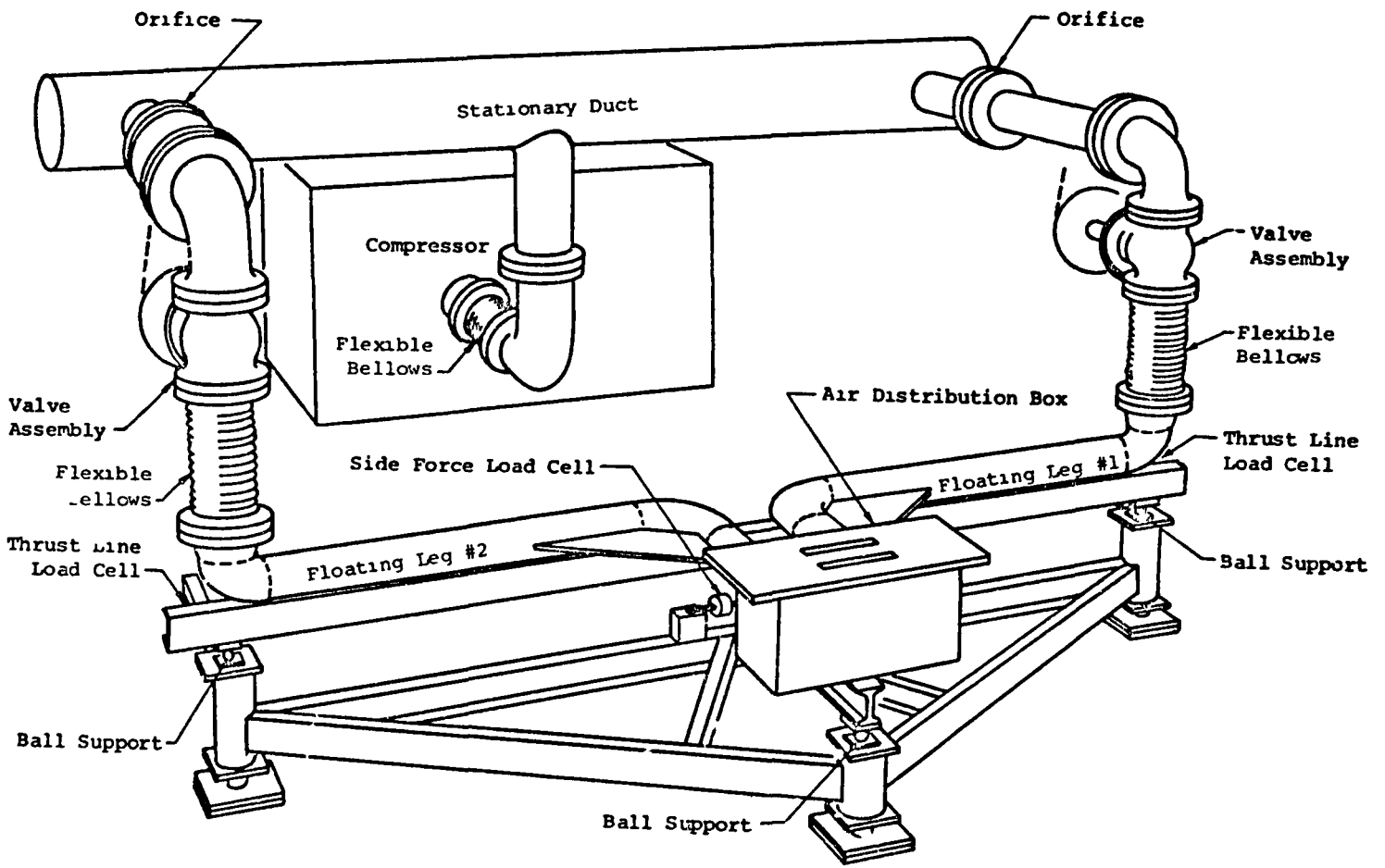

Figure 11. The FDRC static test rig with low pressure air system

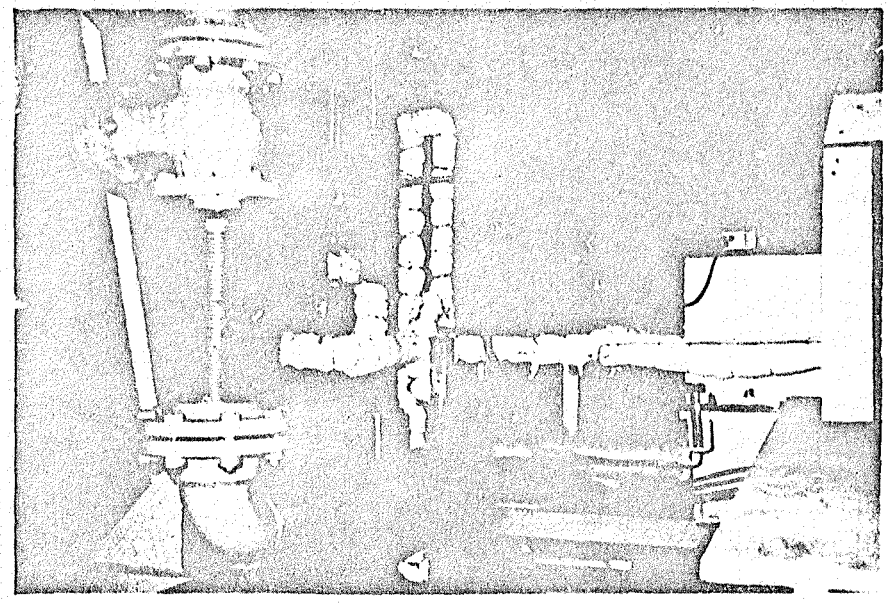

Figure 12. High pressure air supply system

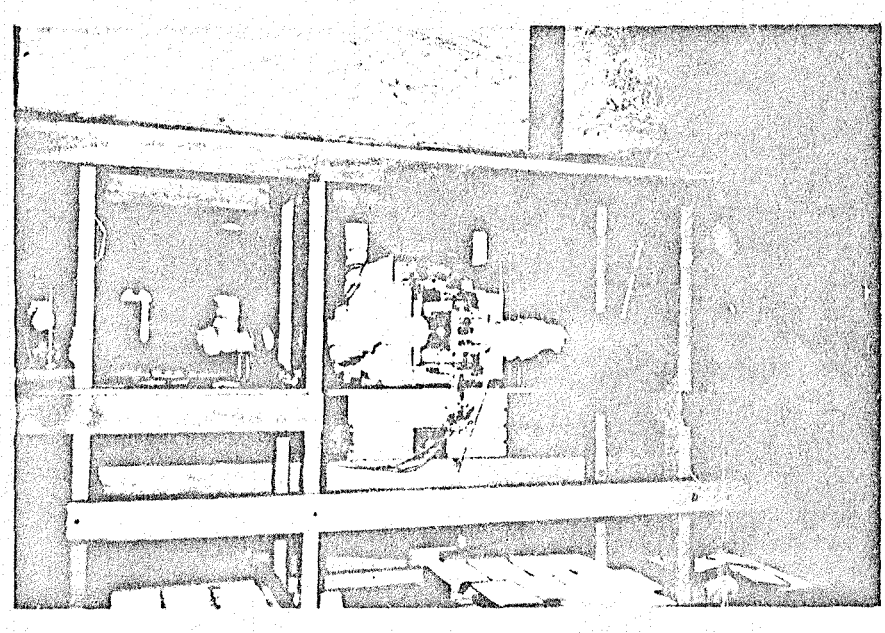

Figure 13. General arrangement for hot gas tests

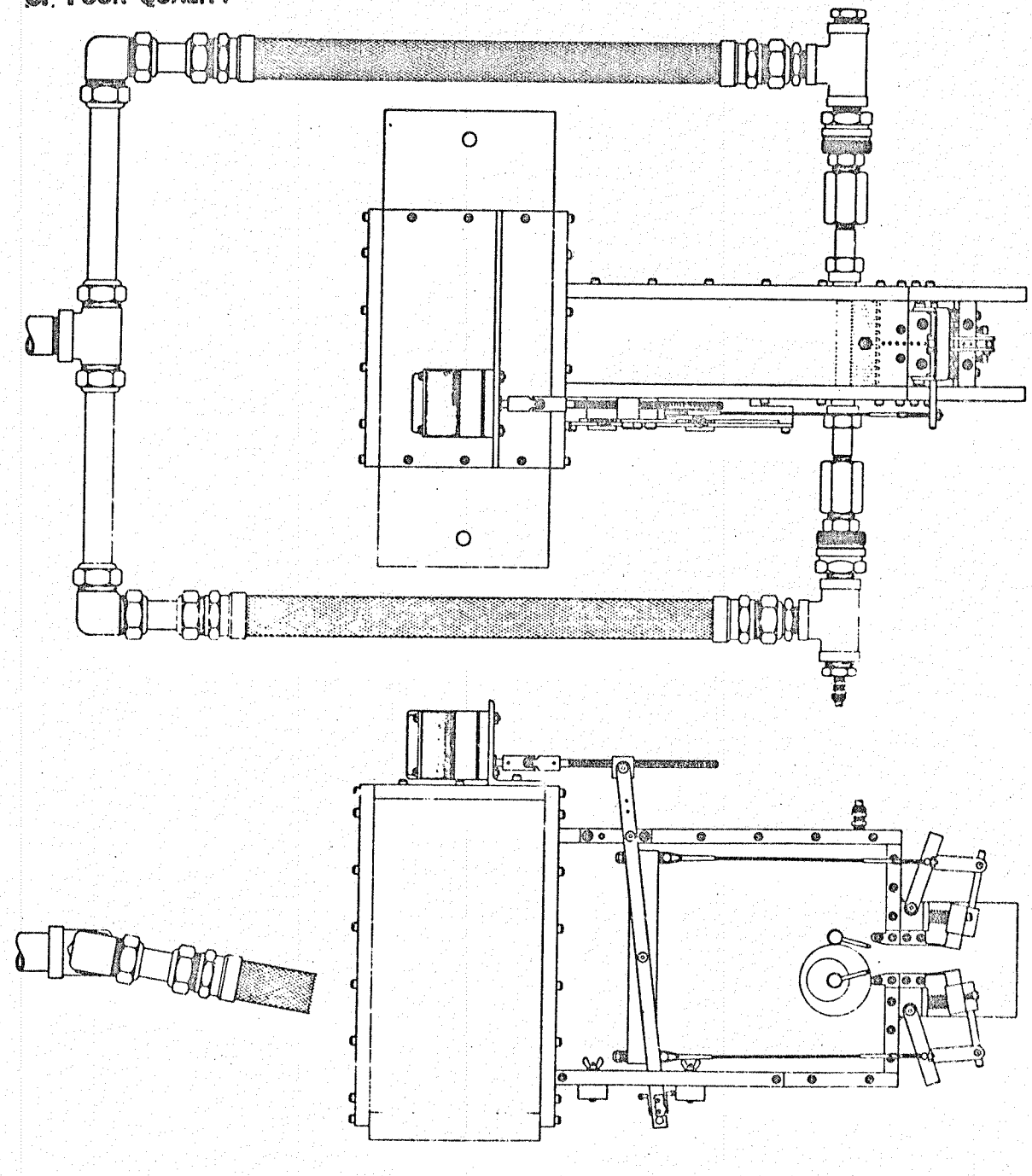

Figure 14. High speed ejector assembly

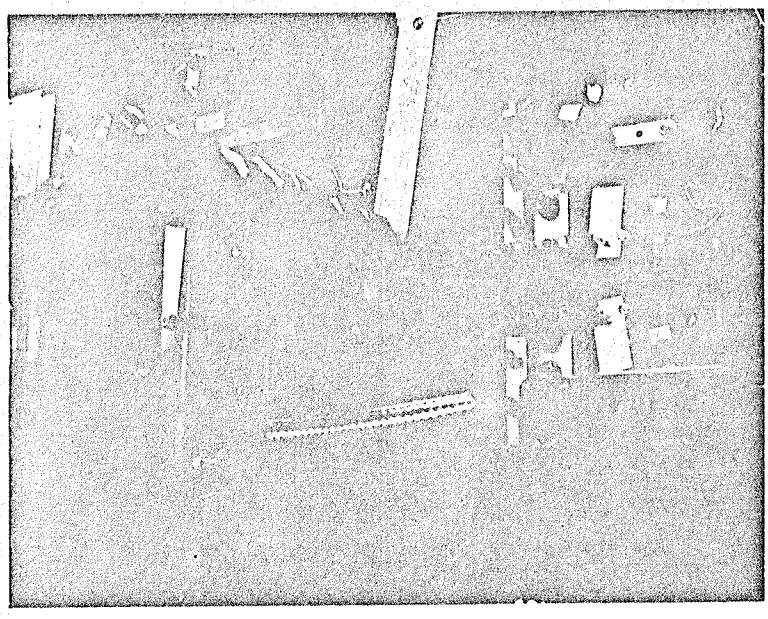

Figure 15. Test model

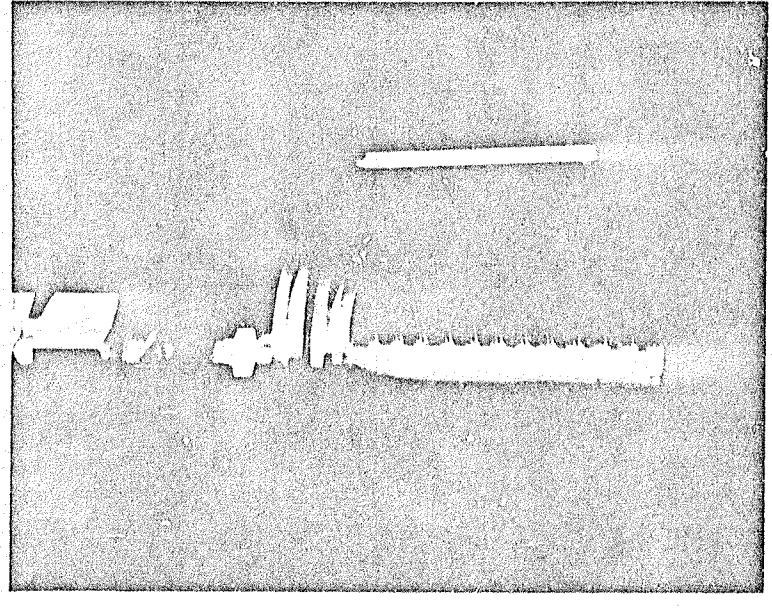

Figure 16. Primary nozzle No. 1

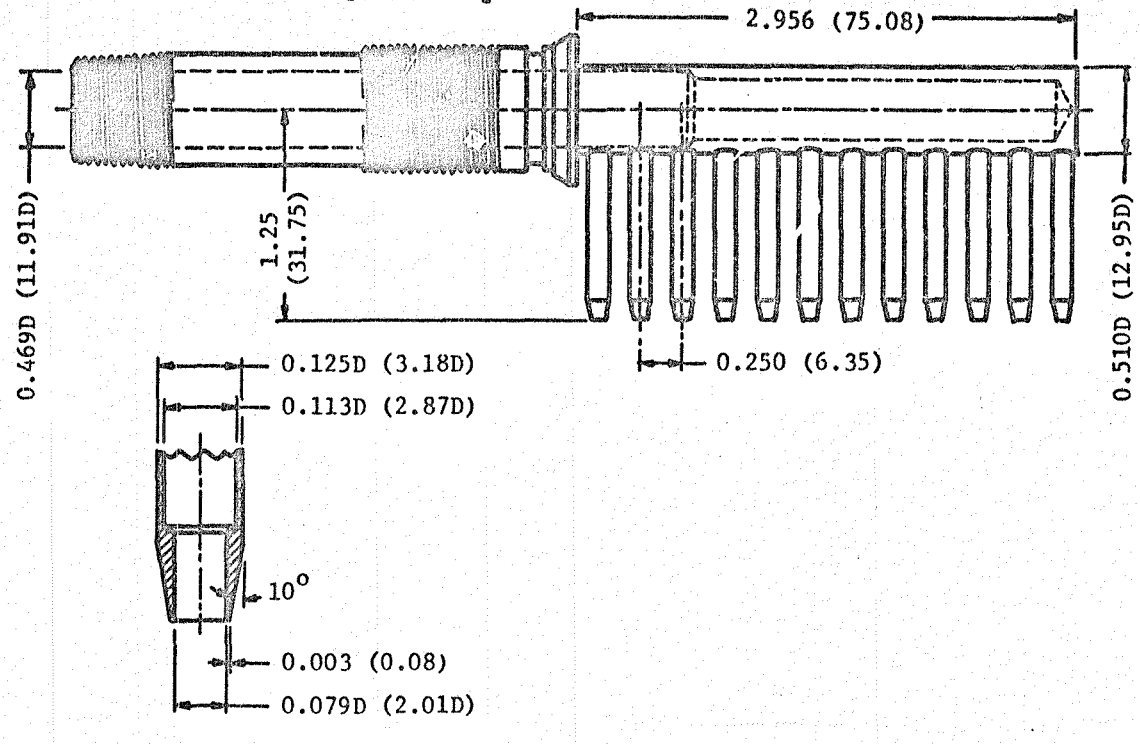

Primary Nozzle No. 1

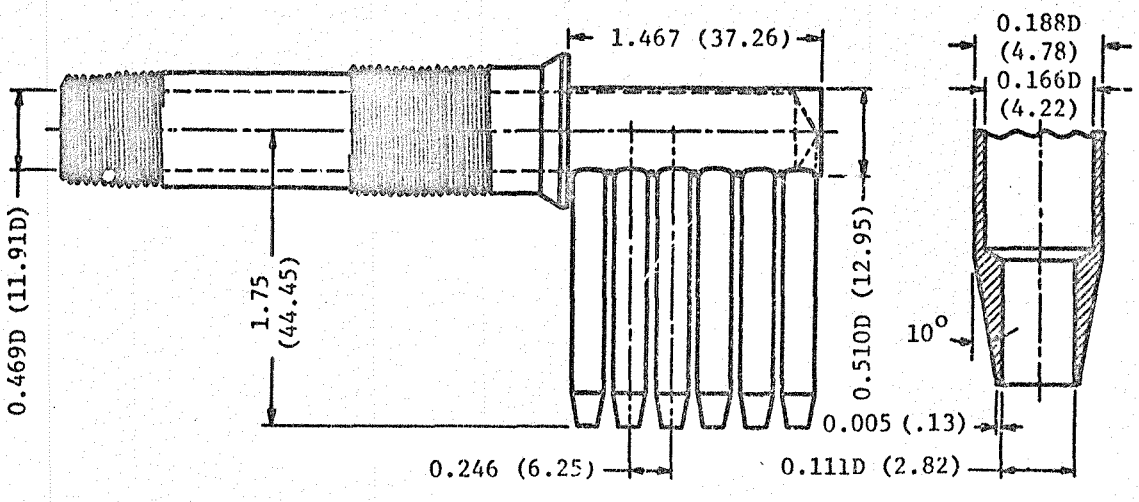

Primary Nozzle No. 2

All dimensions in inches (mm)

Figure 17. Primary Nozzles

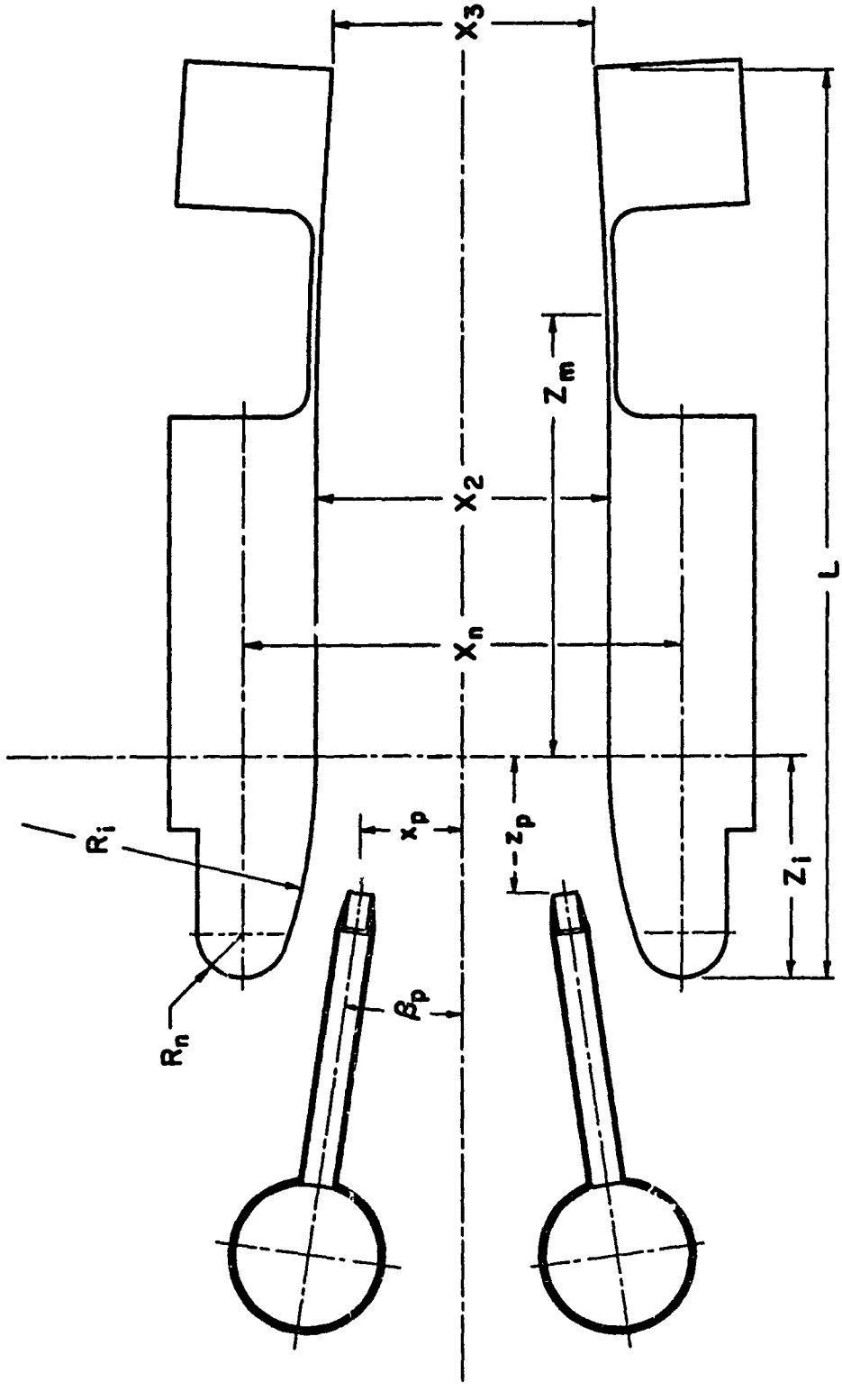

Figure 18. Coordinate System

ORIGINAL PAGE IS
OF POOR QUALITY

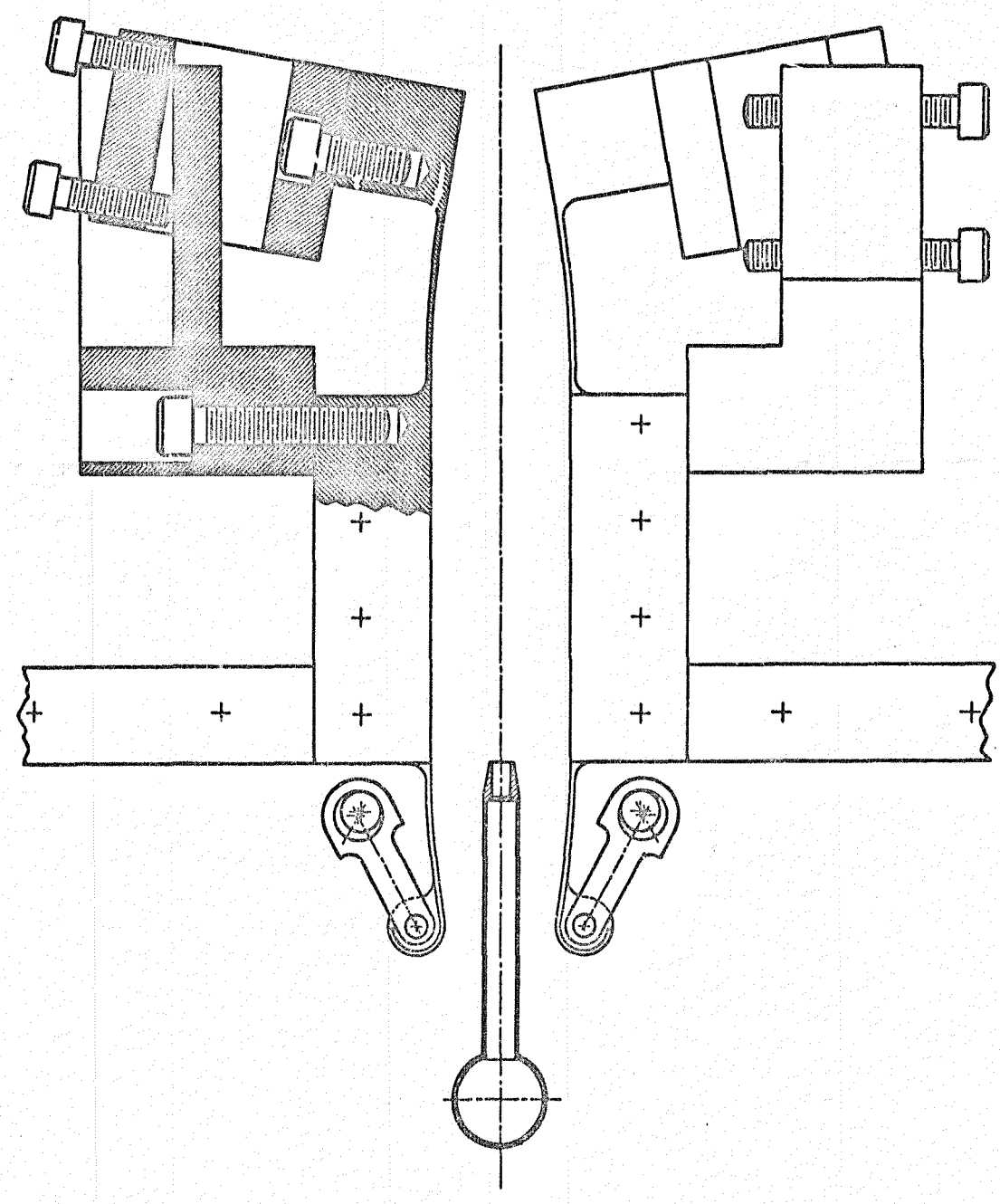

Figure 19. Hot Gas Ejector

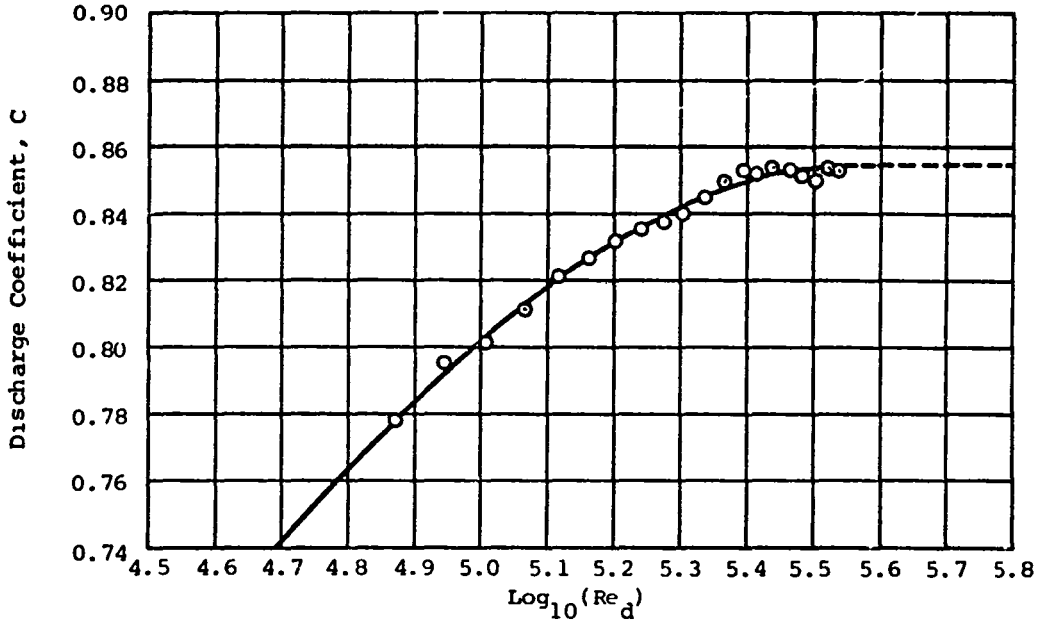

Figure 20. Discharge coefficient of primary nozzle No. 1

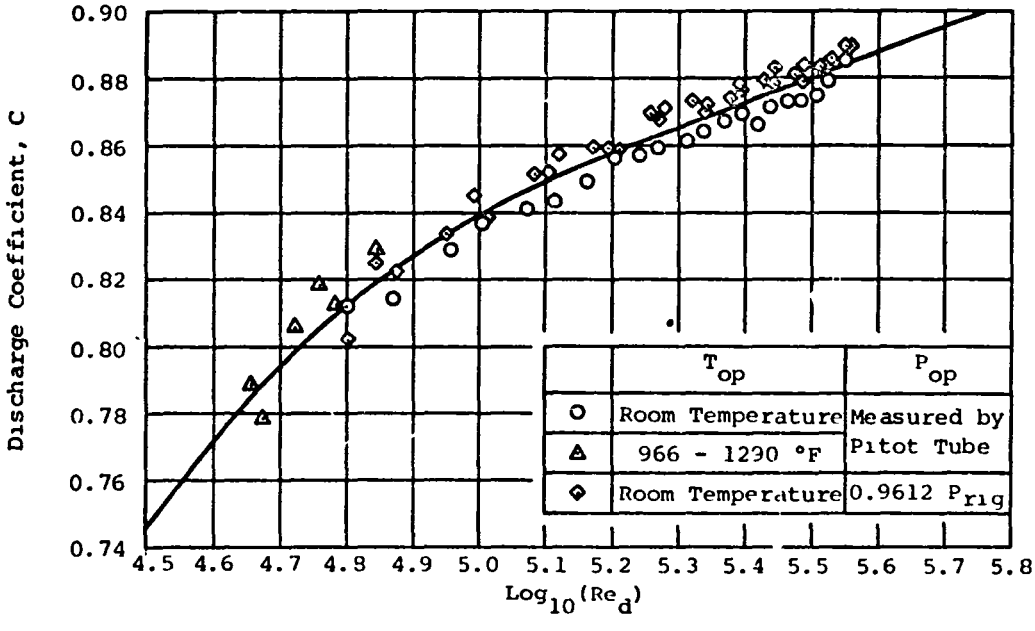

Figure 21. Discharge coefficient of primary nozzle No. 2

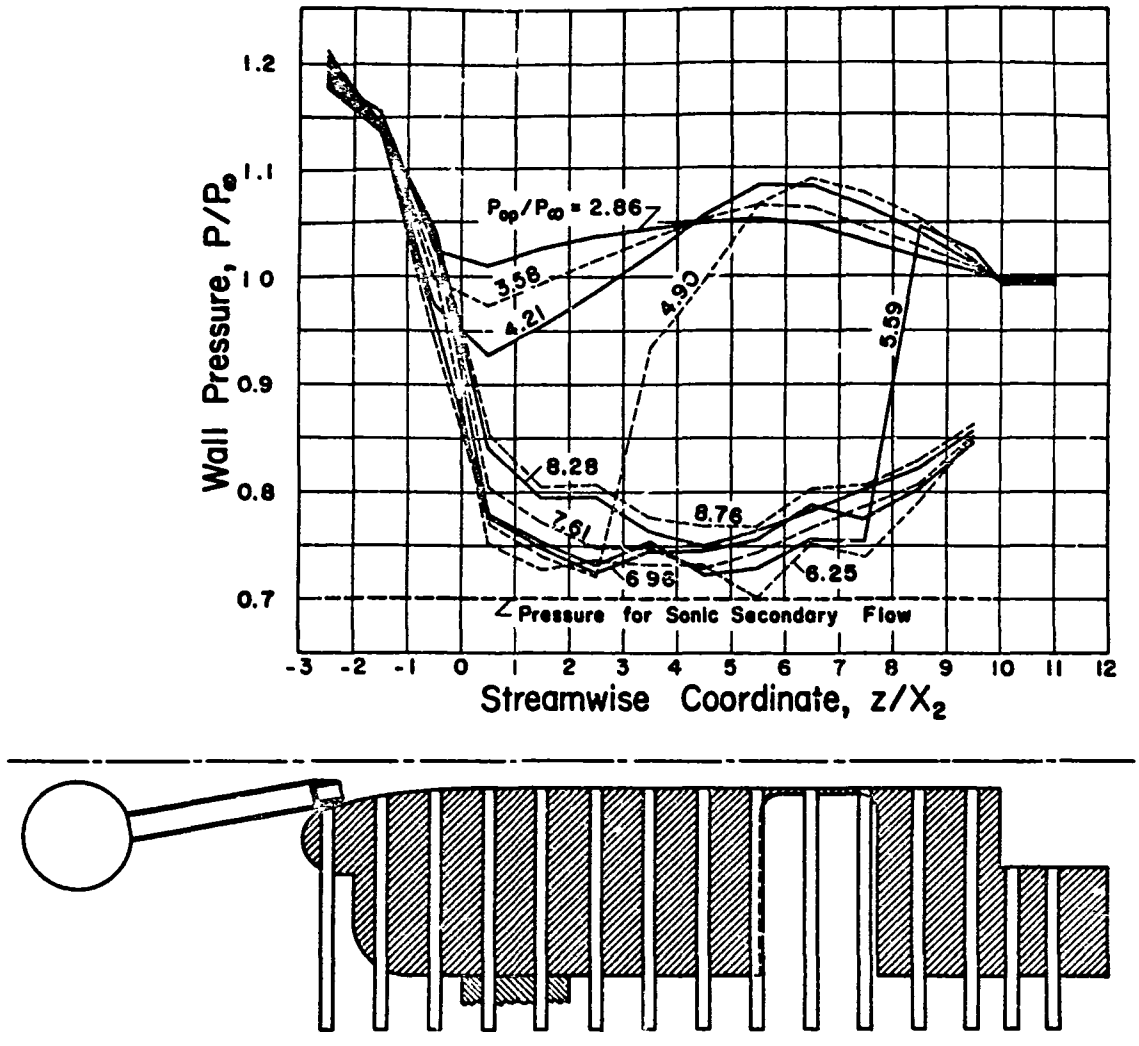

Figure 22. Wall pressure distribution for various primary pressures, X_2 = 0.25" = 6.35 mm, α_* = 7.55, M_∞ = 0.65, X_3/X_2 = 1.01, $T_{op} = T_\infty$

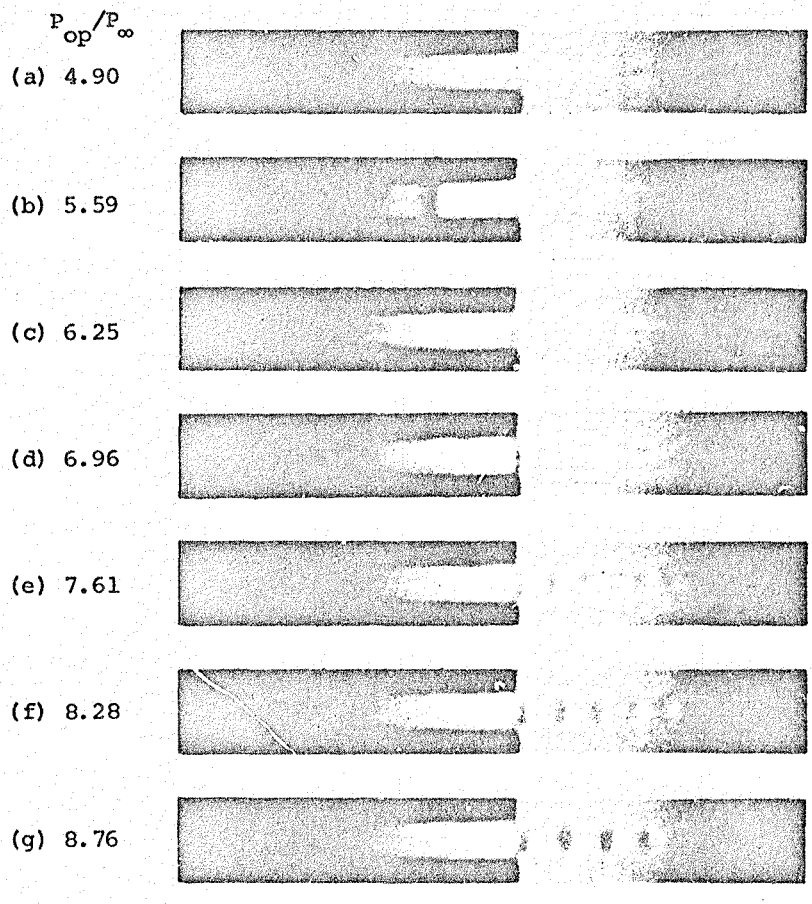

Figure 23. Schlieren photographs of second solution ejectors, $M_{\infty} = 0.65$, $\alpha_{*} = 7.55$, $T_{op} = T_{\infty}$, $X_2 = 0.25" = 6.35$ mm $X_3/X_2 = 1.01$

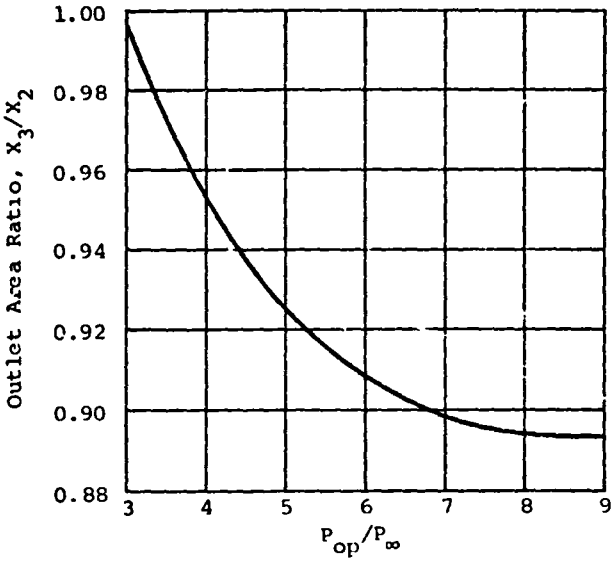

Figure 24. Maximum outlet area ratio of the first solution, $M_\infty = 0.65$, $\alpha_* = 7.55$, $T_{op} = T_\infty$

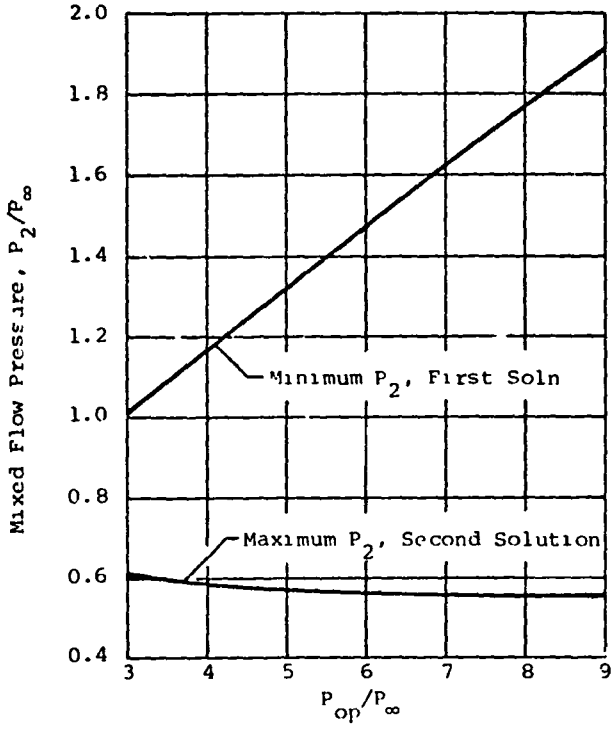

Figure 25. Theoretical limits on the mixed flow pressure, $M_\infty = 0.65$, $\alpha_* = 7.55$, $T_{op} = T_\infty$

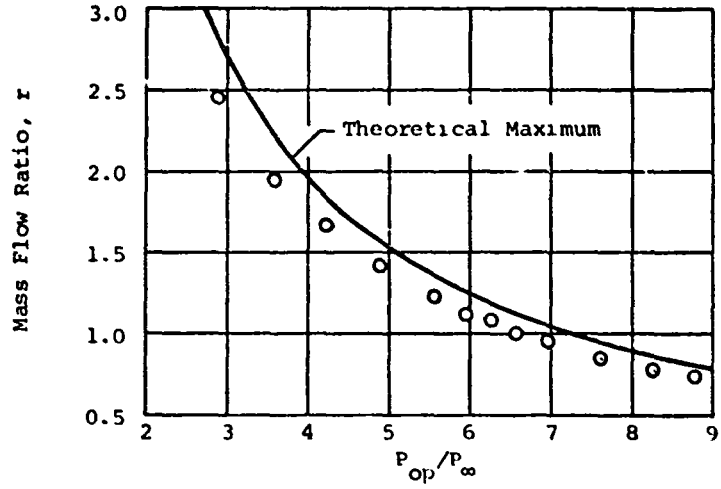

Figure 26. Secondary to primary mass flow ratio, $M_\infty = 0.65$, $\alpha_* = 7.55$, $T_{op} = T_\infty$, $X_3/X_2 = 1.01$

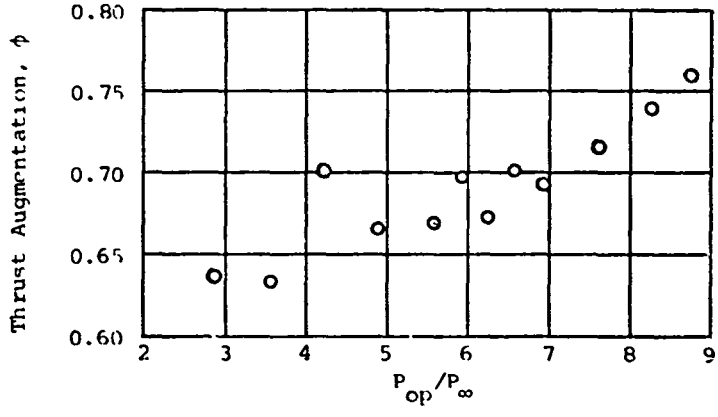

Figure 27. Ejector Performance, $X_2 = 0.25" = 6.35$ mm $M_\infty = 0.65$, $\alpha_* = 7.55$, $T_{op} = T_\infty$, $X_3/X_2 = 1.01$

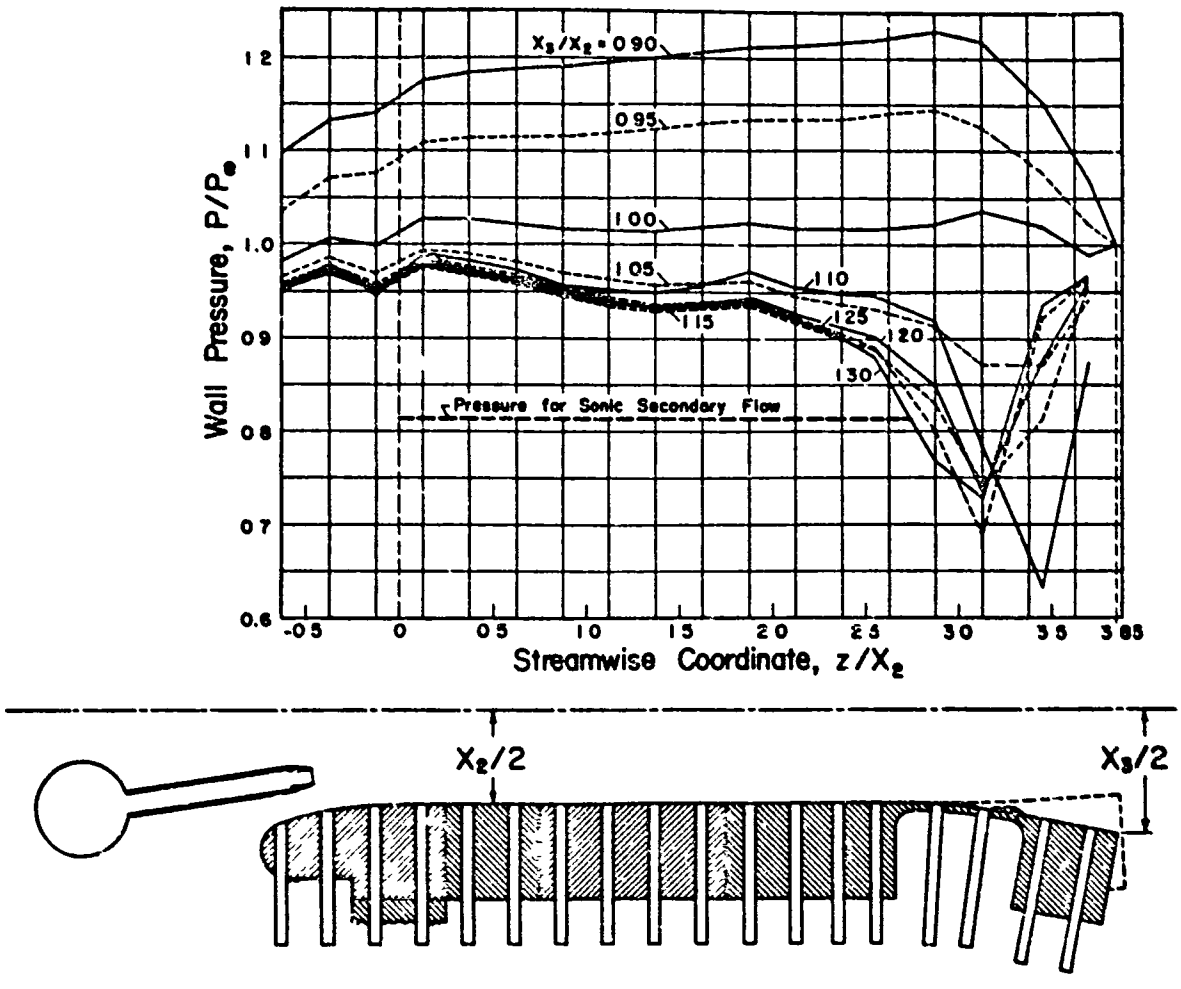

Figure 28. Wall pressure distribution for various outlet area ratios, X_2 = 1" = 25.4 mm, $\alpha_* = 30.2$, $M_\infty = 0.81$, $P_{op}/P_\infty = 5.83$, $T_{op} = T_\infty$

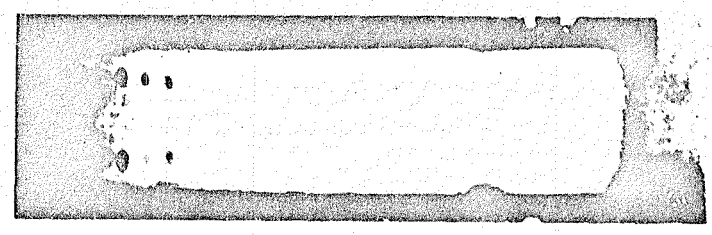

Figure 29. Schlieren photograph of a second solution ejector, $M_\infty = 0.81$, $\alpha_* = 30.2$, $P_{op}/P_\infty = 5.83$, $T_{op} = T_\infty$ $X_2 = 1" = 25.4$ mm, $X_3/X_2 = 1.1$

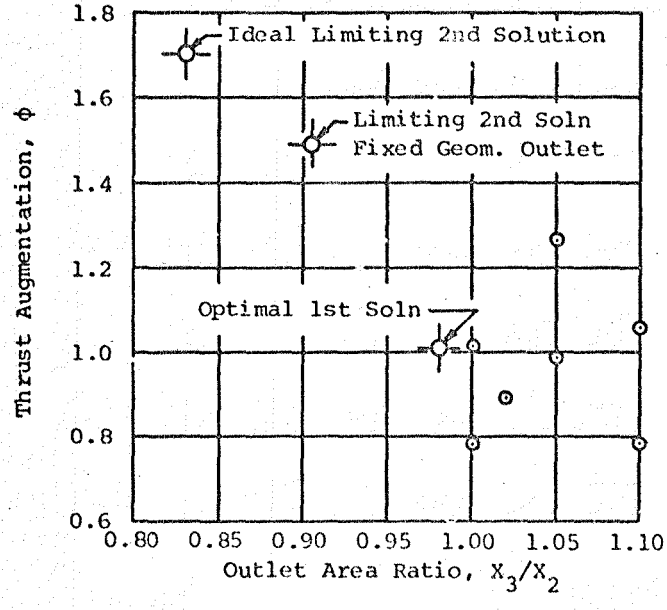

Figure 30. Ejector performance, $X_2 = 1" = 25.4$ mm $M_\infty = 0.81$, $\alpha_* = 30.2$, $P_{op}/P_\infty = 5.88$, $T_{op} = T_\infty$

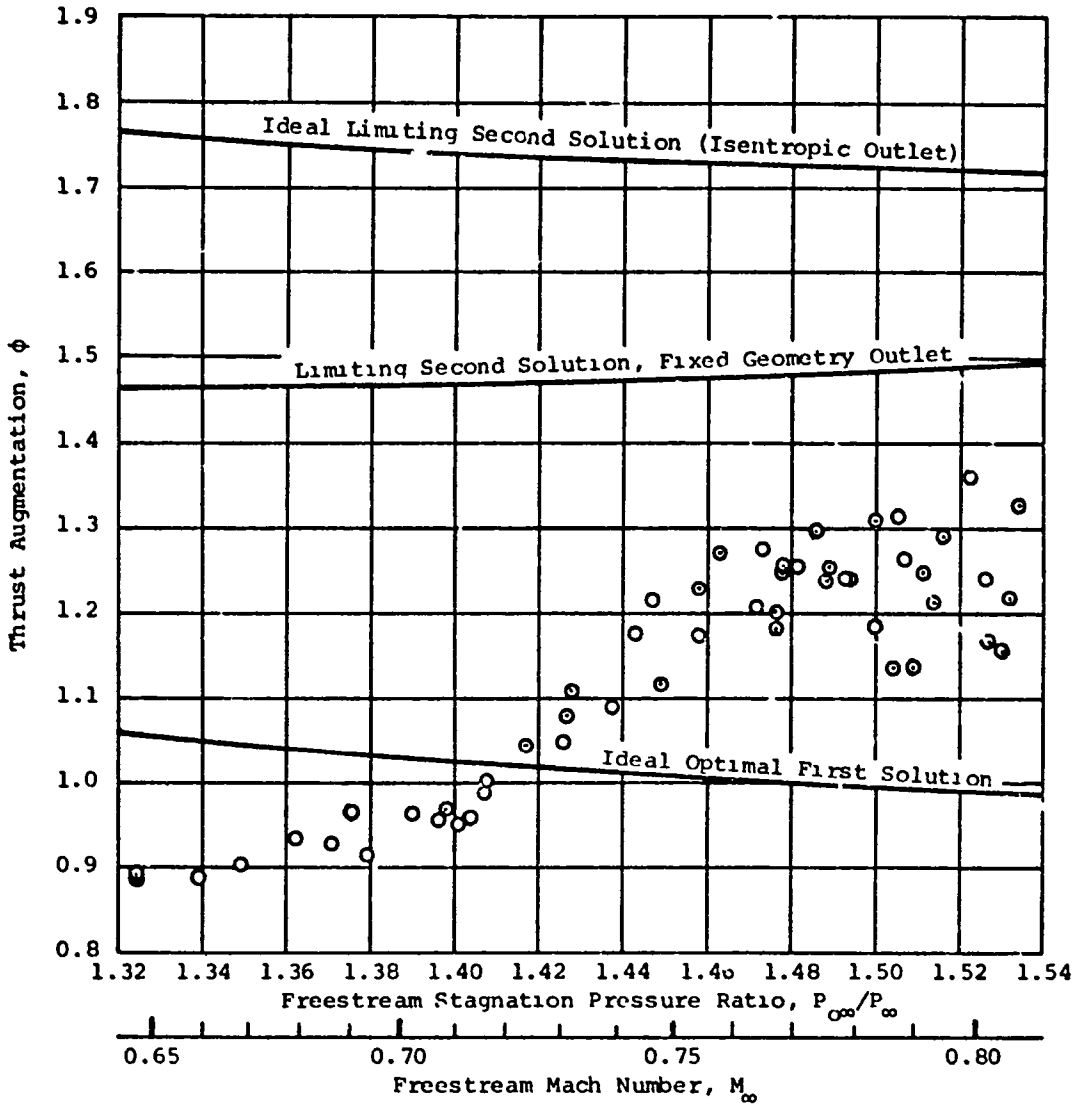

Figure 31. Ejector performance, $P_{op}/P_\infty = 7.65$, $\alpha_* = 30.2$, $T_{op} = T_\infty$

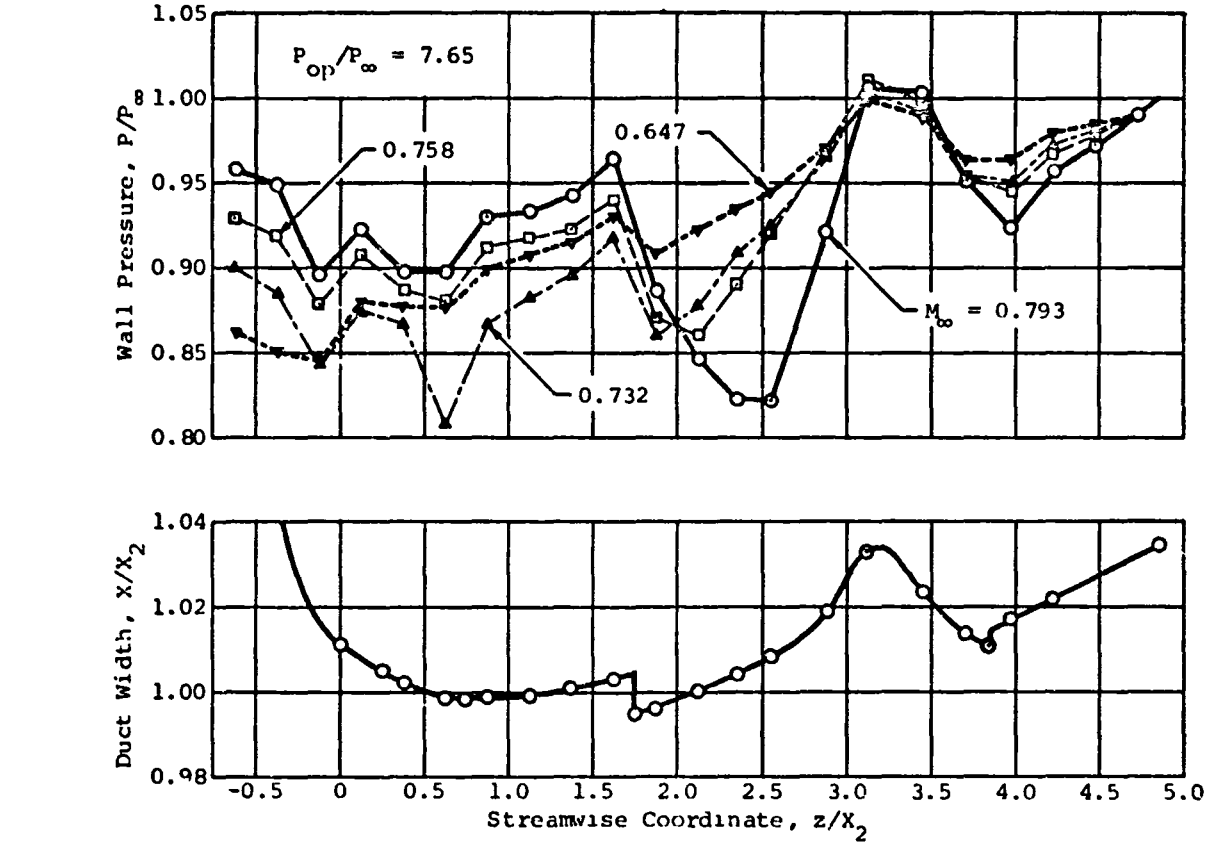

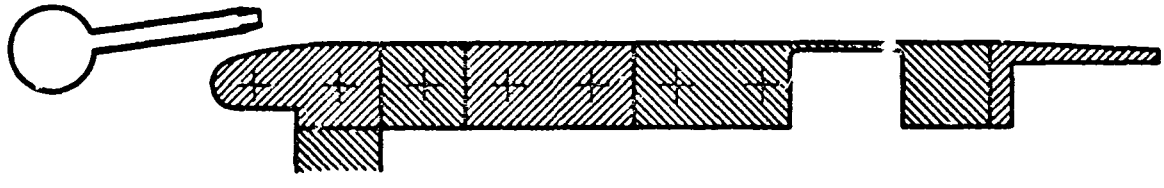

Figure 32. Wall pressure distribution and duct width, P_{op}/P_∞ = 7.65, $\alpha_* = 30.2$, $T_{op} = T_\infty$, X_2 = 1" = 25.4 mm

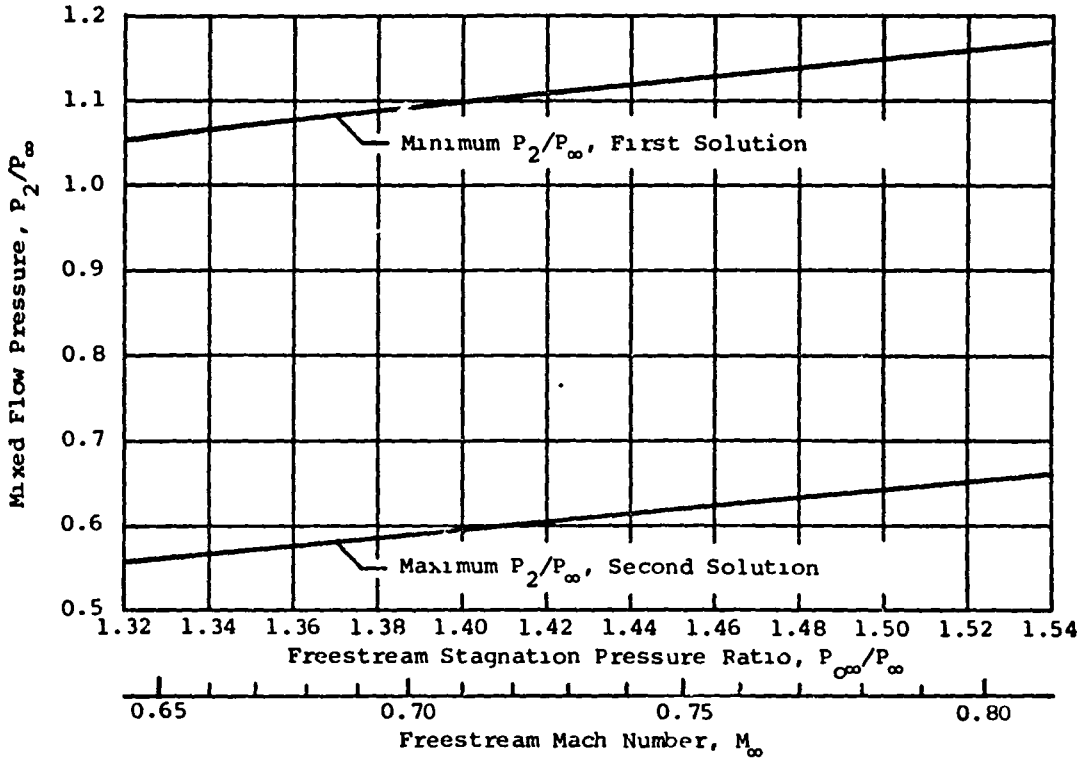

Figure 33. Theoretical limits on the mixed flow pressure, $P_{op}/P_\infty = 7.65$, $\alpha_* = 30.2$, $T_{op} = T_\infty$

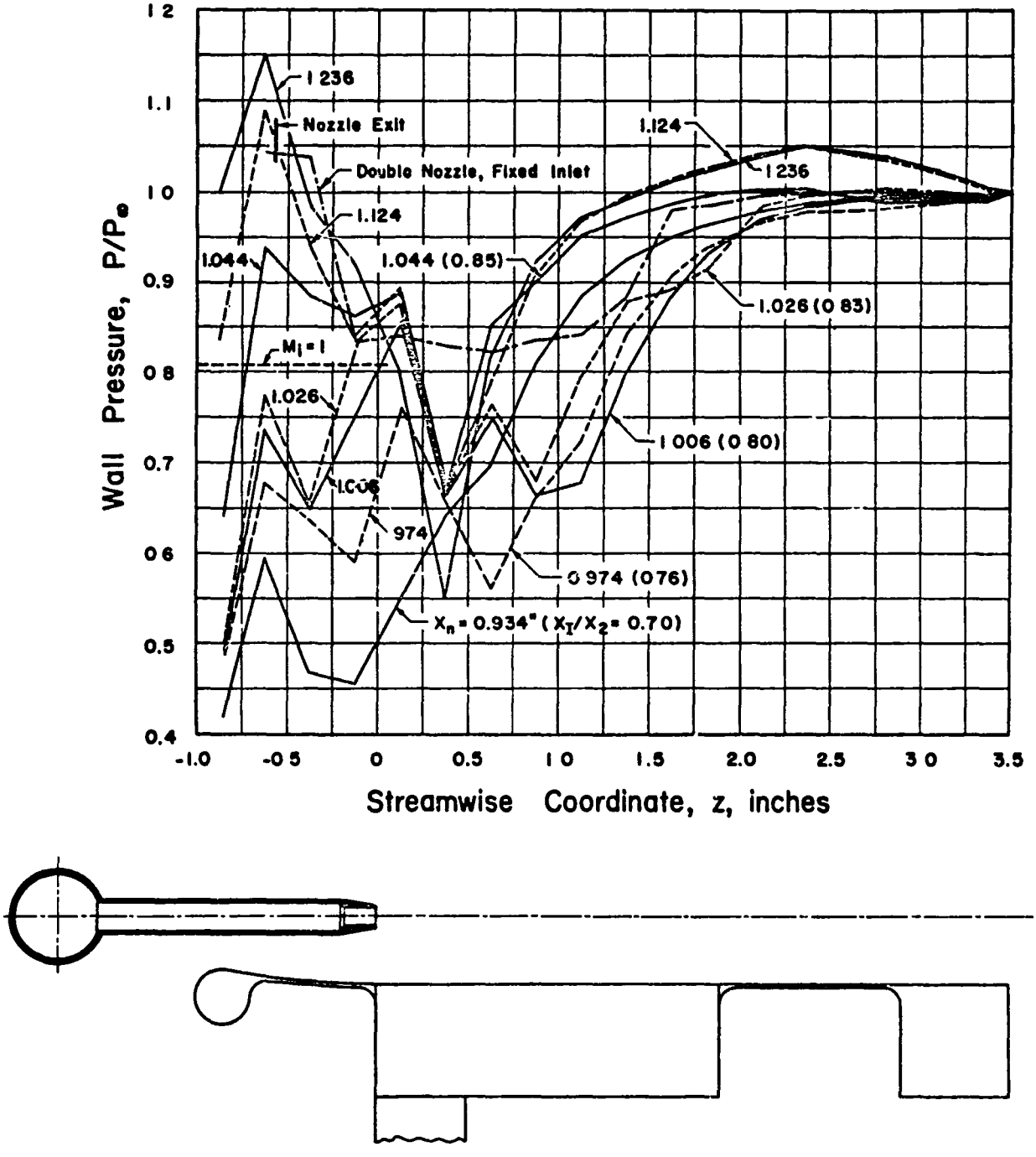

Figure 34. Wall pressure distribution for various inlet settings, $X_2 = 0.744" = 18.9$ mm, $X_3/X_2 = 1.0$, $\alpha_* = 21.8$, $z_p = 0$, $M_\infty = 0.80$, $P_{op}/P_\infty = 8.3$, $T_{op} = T_\infty$

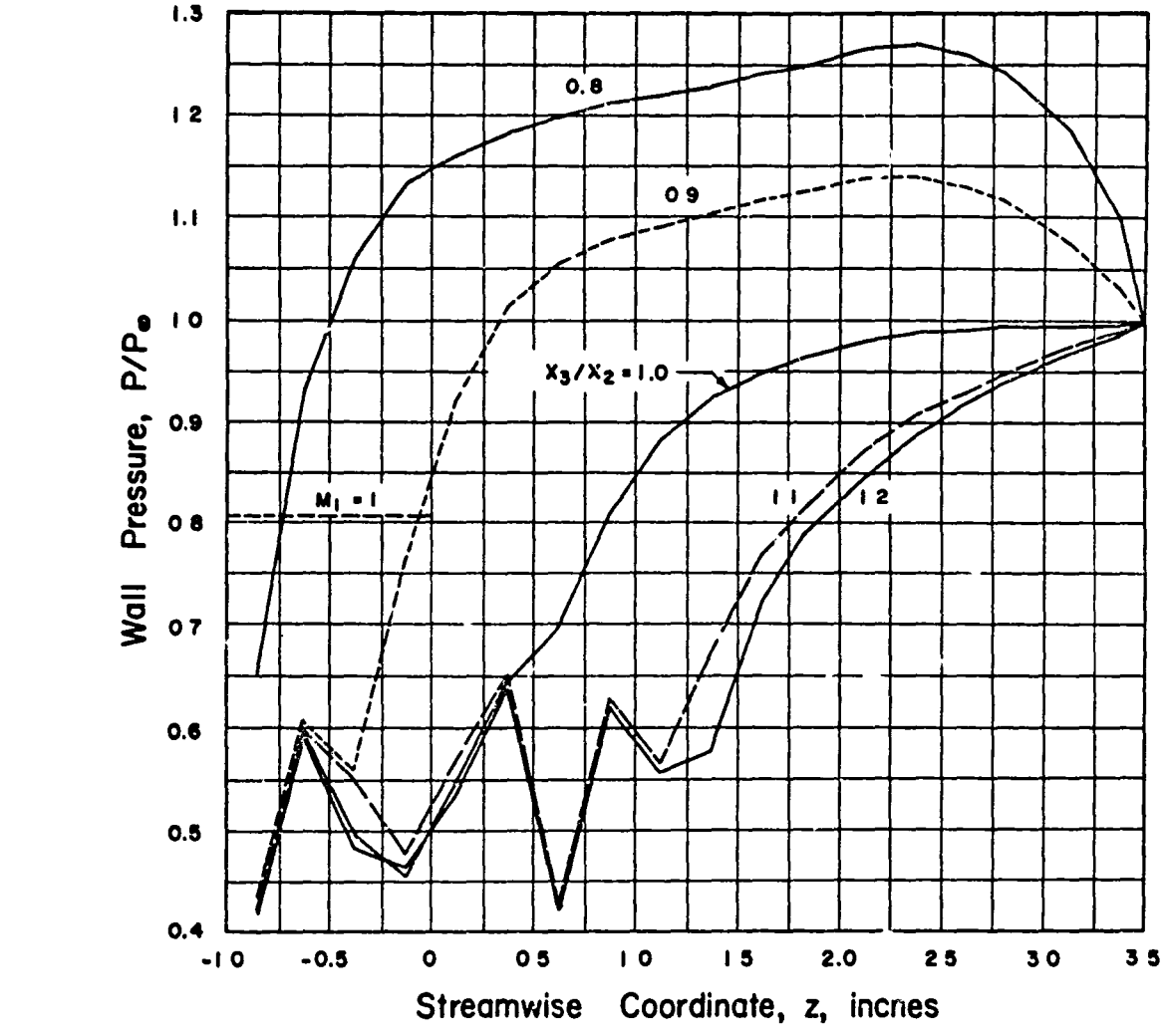

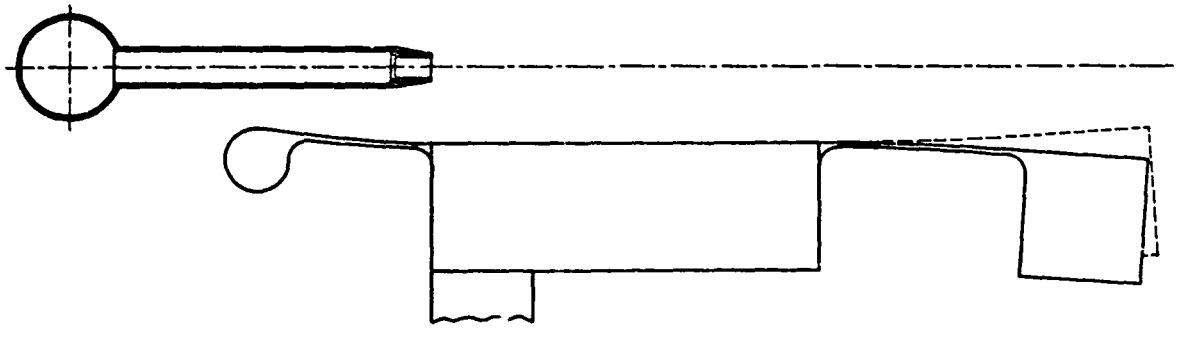

Figure 35. Wall pressure distribution for various outlet area ratios, $X_2 = 0.744" = 18.9$ mm, $X_n = 0.934"$, $\alpha_* = 21.8$, $z_p = 0$, $M_\infty = 0.80$, $P_{op}/P_\infty = 8.3$, $T_{op} = T_\infty$

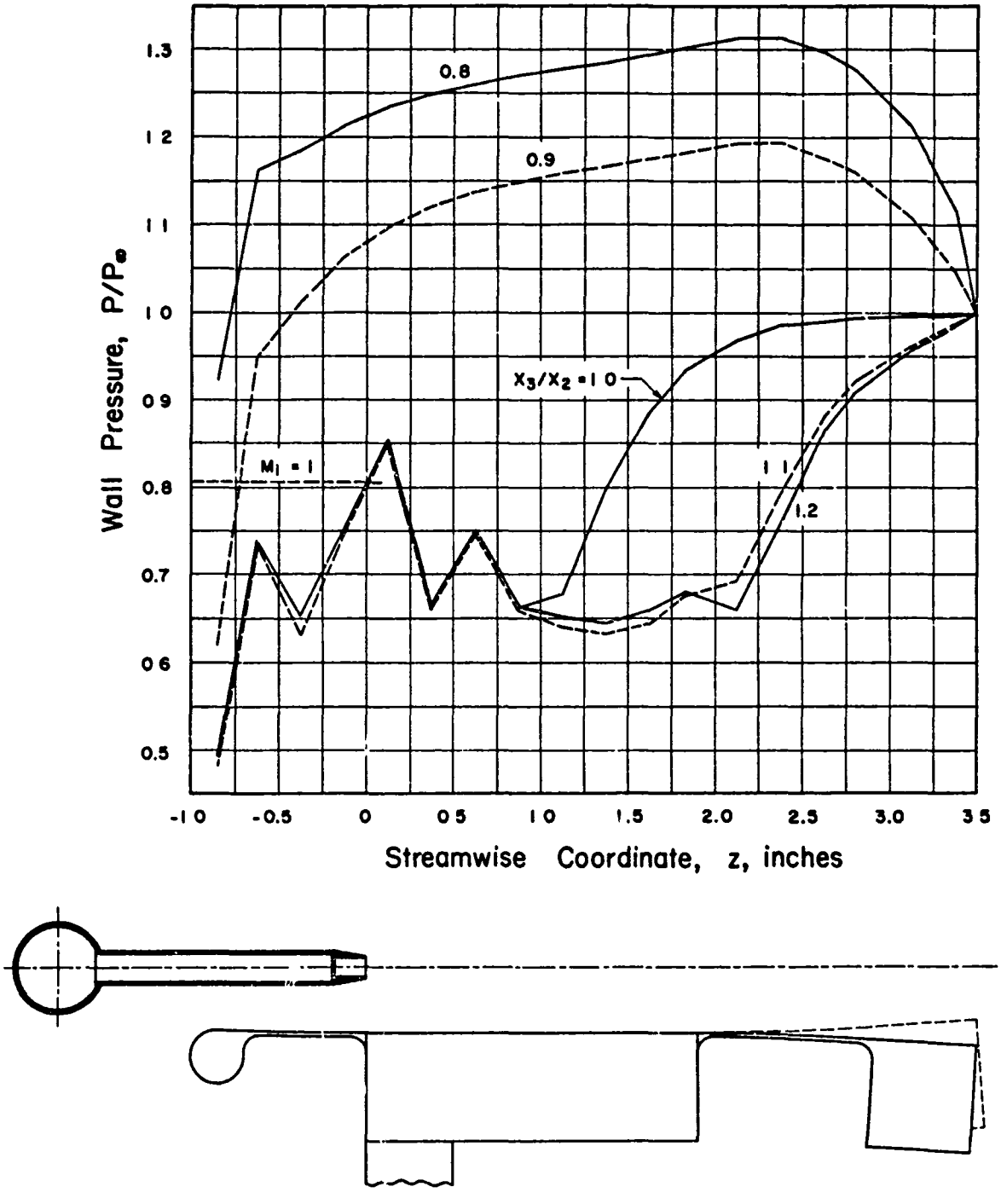

Figure 36. Wall pressure distribution for various outlet area ratios, X_2 = 0.744" = 18.9 mm, X_n = 1.006", α_* = 21.8, z_p = 0, M_∞ = 0.80, P_{op}/P_∞ = 8.3, $T_{op} = T_\infty$

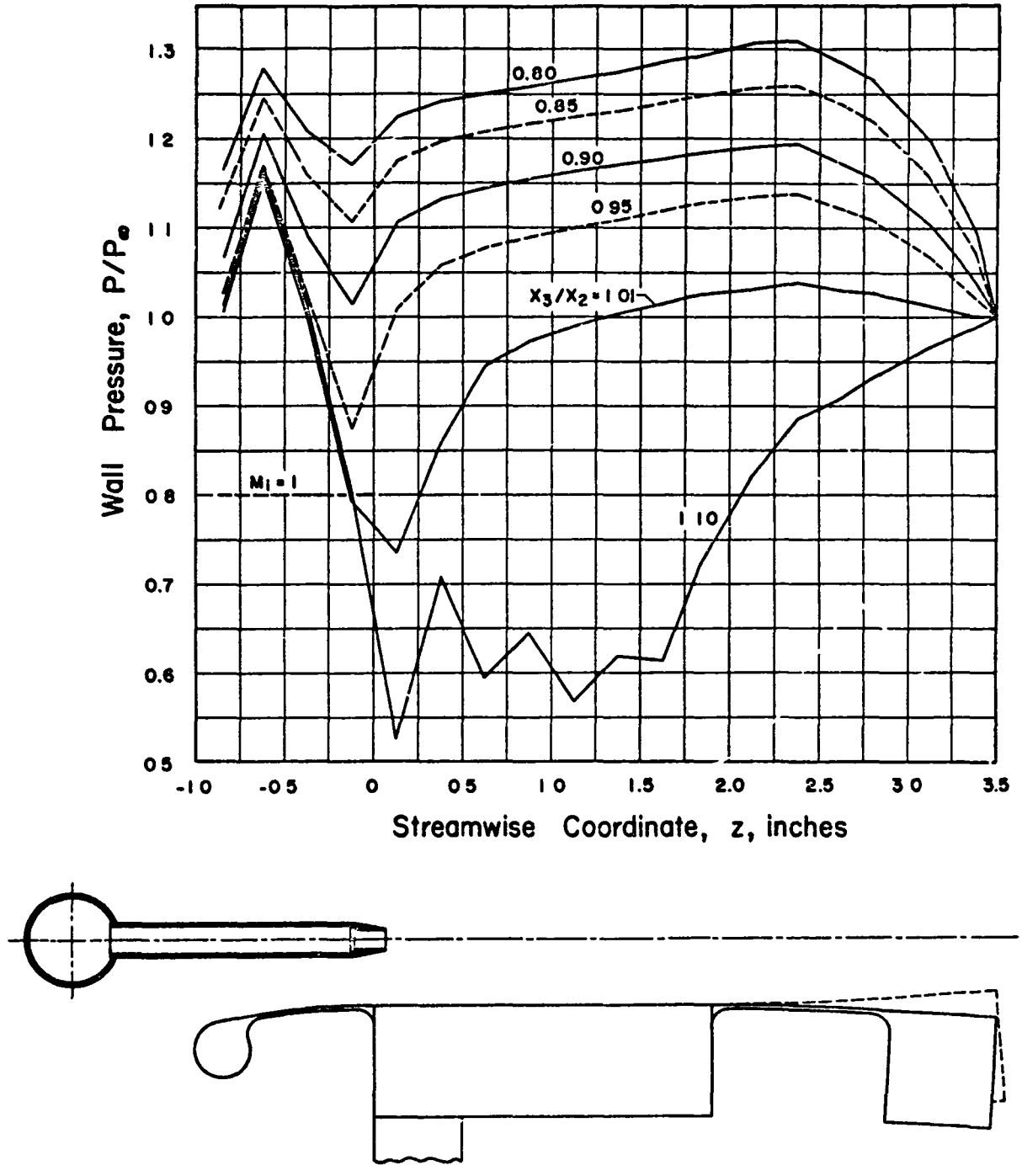

Figure 37. Wall pressure distribution for various outlet area ratios, X_2 = 0.744" = 18.9 mm, X_n = 1.236", α_* = 22, z_p = 0.065", M_∞ = 0.79, P_{op}/P_{to} = 6.24, $T_{op} = T_\infty$

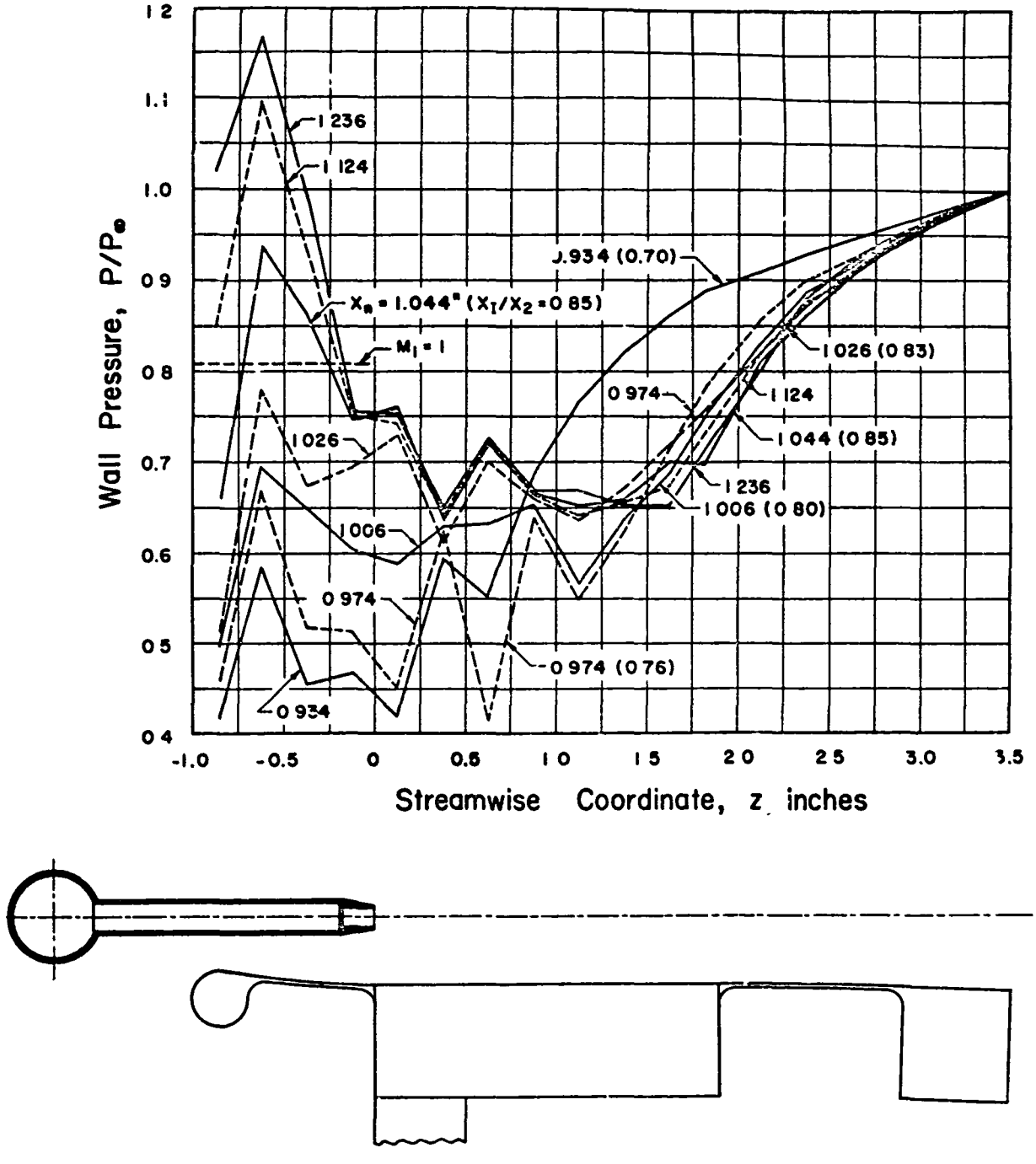

Figure 38. Wall pressure distribution for various inlet settings, X_2 = 0.744" = 18.9 mm, X_3/X_2 = 1.1, α_* = 23.3, z_p = 0, M_∞ = 0.80, P_{op}/P_∞ = 6.1, T_{op}/T_∞ = 3.23

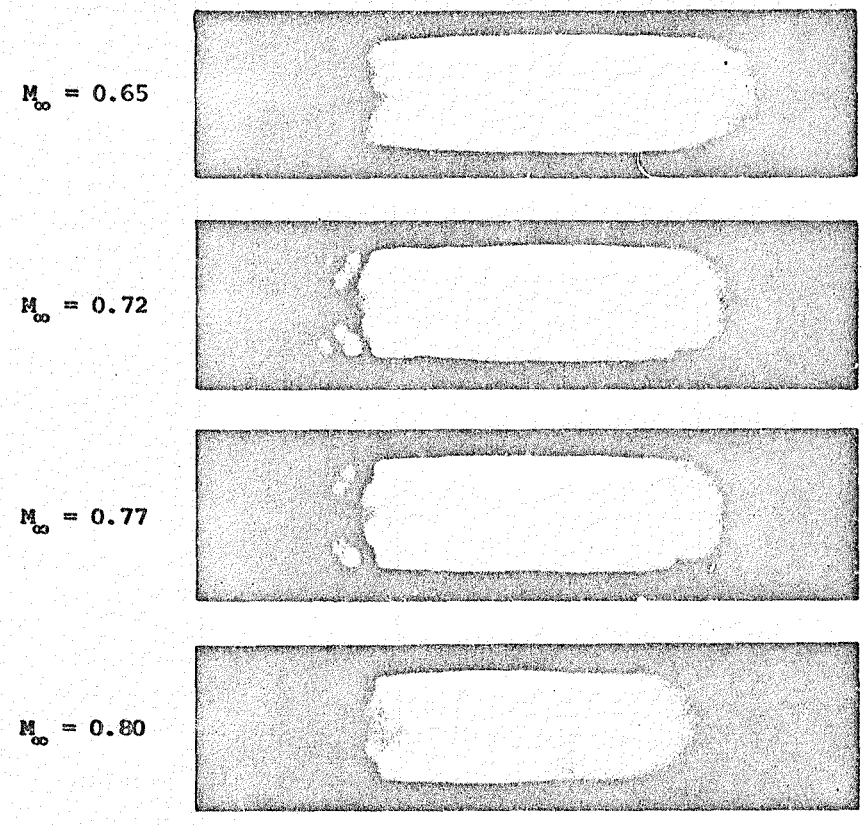

Figure 39. Schlieren photographs of the hot gas ejector, X_2 = 0.744" = 18.9 mm, X_3/X_2 = 1.0, α_* = 21.8, P_{op}/P_∞ = 8.3, $T_{op} = T_\infty$, X_n = 1.124", z_p = 0

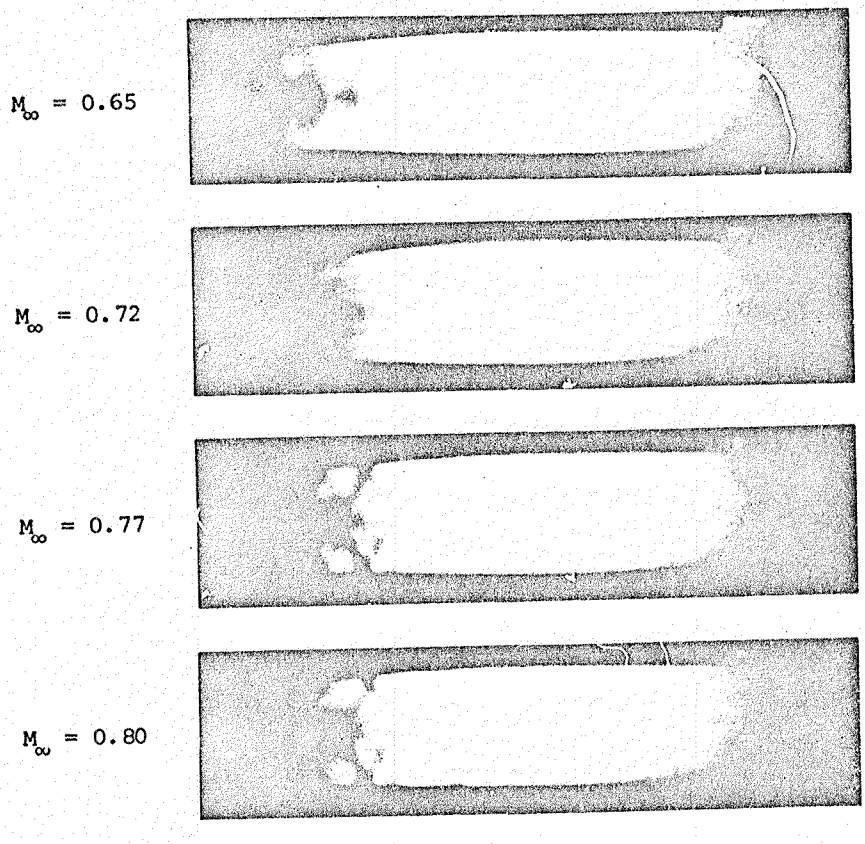

Figure 40. Schlieren photographs of the hot gas ejector, X_2 = 0.744" = 18.9 mm, X_3/X_2 = 1.0, α_* = 23.3, P_{op}/P_∞ = 6.1, T_{op}/T_∞ = 3.23, X_n = 1.124", z_p = 0

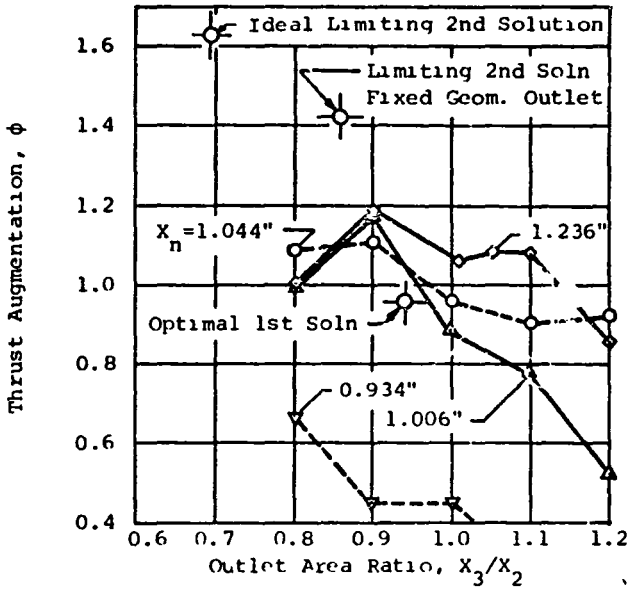

Figure 41. Ejector performance, X_2 = 0.744", z_p = 0
M_∞ = 0.8, α_* = 21.8, P_{op}/P_∞ = 8.3, T_{op}/T_∞ = 1

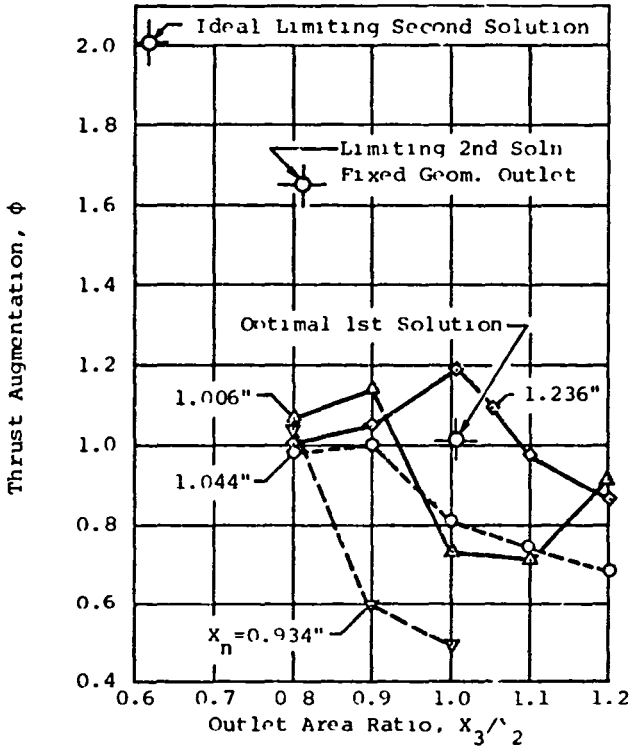

Figure 42. Ejector performance, X_2 = 0.744", z_p = 0
M_∞ = 0.8, α_* = 23.3, P_{op}/P_∞ = 6.' T_{op}/T_∞ = 3.23

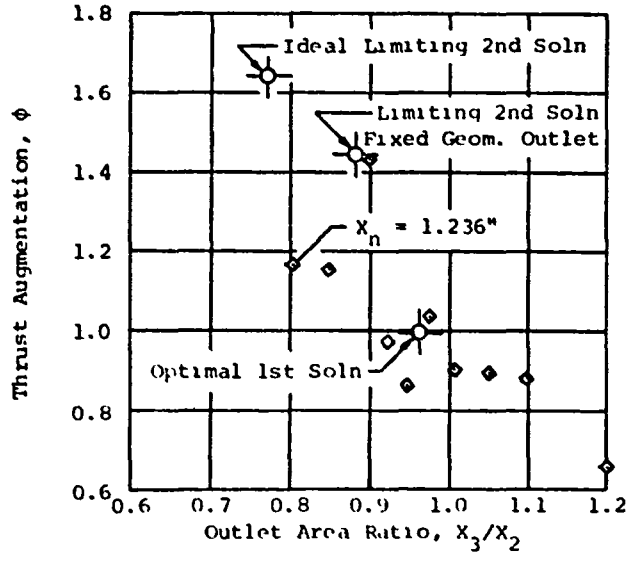

Figure 43. Ejector performance, X_2 = 0.744", z_p = 0
M_∞ = 0.8, α_* = 22, P_{op}/P_∞ = 6.24, T_{op}/T_∞ = 1

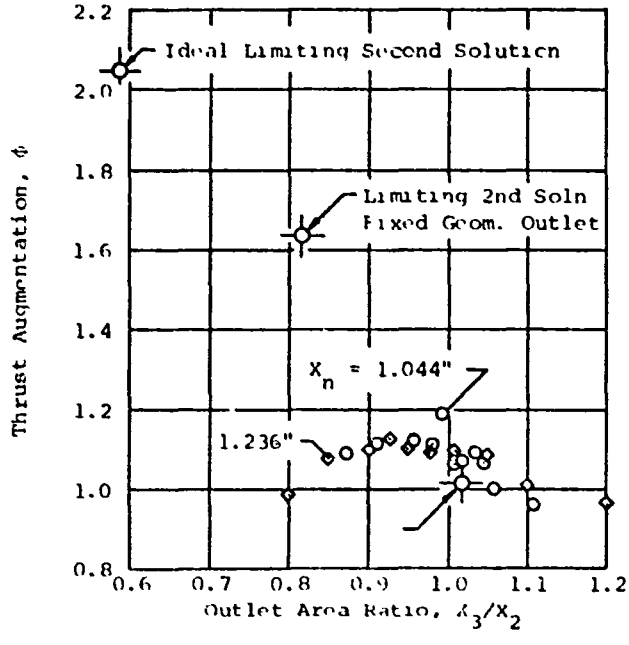

Figure 44. Ejector Performance, X_2 = 0.744", z_p = 0
M_∞ = 0.72, α_* = 23 3, P_{op}/P_∞ = 6.10, T_{op}/T_∞ = 3.23

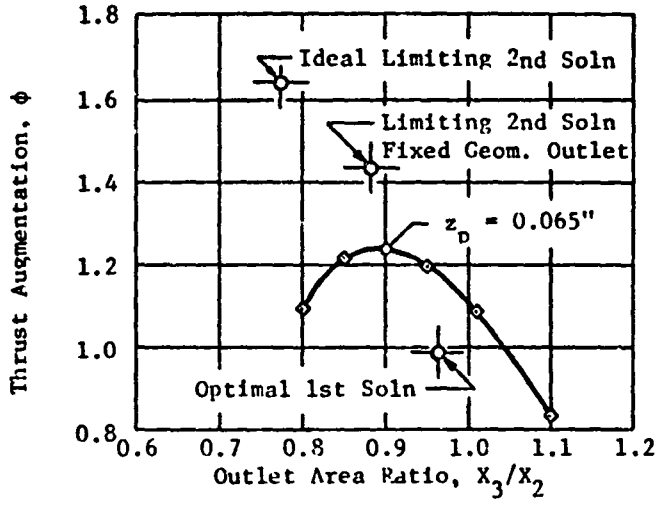

Figure 45. Ejector Performance, X_2 = 0.744", X_n = 1.236"
M_∞ = 0.79, α_* = 22, P_{op}/P_∞ = 6.24, T_{op}/T_∞ = 1

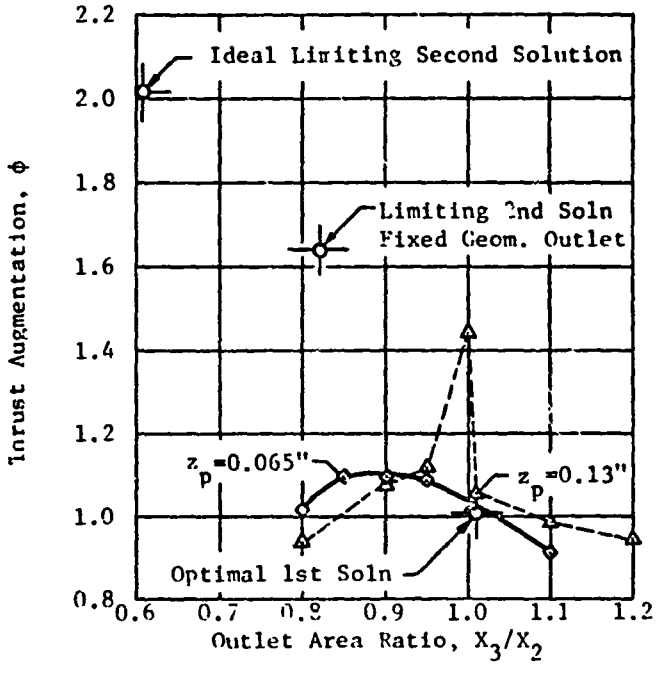

Figure 46. Ejector Performance, X_2 = 0.744", X_n = 1.236"
M_∞ = 0.77, α_* = 23.3, P_{op}/P_∞ = 6.10, T_{op}/T_∞ = 3.23

APPENDIX A

Tare Forces of the FDRC Static Test Rig

The experimental approach was discussed in "Data Reduction." The coordinate system is presented on Figure A-1. The general arrangement of the test rig was shown on Figure 11. Special symbols used in this Appendix will be defined as they appear.

Basic Force System

$$Fx = -0.00719038\ F1 + 0.00016650\ F1^2 + 0.00547198\ F2 - 0.00009834\ F2^2 + 1.00825861\ F5 - 0.00014203\ F5^2 + Dfx$$

$$Fy = 1.00314732\ F1 + 0.00031097\ F1^2 + 1.01516450\ F2 + 0.00014718\ F2^2 + 0.00423935\ F5 + 0.00008434\ F5^2 + Dfy$$

$$Mo = -58.43137304\ F1 - 0.01986357\ F1^2 + 58.87868543\ F2 - 0.00114932\ F2^2 + 1.43581856\ F5 + 0.01075702\ F5^2$$

where F1, F2, and F5 are load cell readings after correction for pressure tares, and Dfx and Dfy are temperature corrections of the high pressure system,

$$F1 = F01 - (F10 + F11 + F12 + F13 + F14)$$

$$F2 = F02 - (F20 + F21 + F22 + F23 + F24)$$

$$F5 = F05 - (F50 + F51 + F52 + F53 + F54)$$

where,

F01, F02, and F05 are load cell readings.

F10, F20, and F50 are low pressure tares due to stationary duct.

F11, F21, and F51 are low pressure tares due to floating Leg #1.

F12, F22, and F52 are low pressure tares due to floating Leg #2.

F13, F23, and F53 are low pressure tares due to interference of floating Leg #1 and floating Leg #2.

F14, F24, and F54 are high pressure tares due to high pressure air supply system.

Low Pressure Tares due to Stationary Duct

P = Pa = characteristic pressure (psig)

Pa = Pm - 1.111 Dp

Pm = averaged maximum system pressure

Maximum System Pressure
= Downstream Orifice Pressure + 1.68 Dp (open leg)
= Downstream Orifice Pressure + Dp (if > 0) (closed leg)

Dp = diffcrential pressure of the orifice if only one leg is open
= averaged differential pressure of the orifices if both legs are open

i) F10

$P \leq 6.82045$	$F10 = -0.04541\ P$
$6.82045 < P$	$F10 = -2.47405 + 0.31733\ P$

ii) F20

$P \leq 4.84644$	$F20 = -0.06468\ P - 0.01822\ P^2$
$4.84644 < P \leq 7.15508$	$F20 = 7.62996 - 0.69564\ P$
$7.15508 < P$	$F20 = 9.54971 - 1.66275\ P$

iii) F50

$P \leq 4.81921$	$F50 = 0.11409\ P$
$4.81921 < P \leq 7.27855$	$F50 = -1.80624 + 0.48889\ P$
$7.27855 < P$	$F50 = -5.83397 + 1.04226\ P$

Low Pressure Tares due to Floating Leg #1

P = Pb = characteristic pressure (psig)
= Downstream Orifice Pressure + 0.2372 Dp (open leg)
= Secondary Plenum Pressure (closed leg)

Dp = differential pressure of the orifice

i) F11

$P \leq 4.27437$	$F11 = 0.08019 - 0.47774\ P + 0.02942\ P^2$
$4.27437 < P \leq 6.32031$	$F11 = 1.51797 - 1.05134\ P + 0.08492\ P^2$
$6.32031 < P$	$F11 = -8.28792 + 1.76933\ P - 0.11589\ P^2$

ii) F21

$P \leq 5.51747$	$F21 = -0.05392\ P - 0.00931\ P^2$
$5.51747 < P \leq 6.42659$	$F21 = 1.66684 - 0.40739\ P$
$6.42659 < P \leq 7.10424$	$F21 = 6.93735 - 1.22750\ P$
$7.10424 < P$	$F21 = 3.82575 - 1.43777\ P + 0.09125\ P^2$

iii) F51

$P \leq 4.99108$	$F51 = 0.05727 - 0.73542\ P - 0.01293\ P^2$
$4.99108 < P \leq 7.23443$	$F51 = 2.04714 - 1.19864\ P$
$7.23443 < P$	$F51 = -8.51076 + 2.06184\ P - 0.24896\ P^2$

Low Pressure Tares due to Floating Leg #2

P = Pc = characteristic pressure (psig)
= Downstream Orifice Pressure + 0.2372 Dp (open leg)
= Secondary Plenum Pressure (closed leg)

Dp = differential pressure of the orifice

i) F12

$P \leq 5.37941$	$F12 = -0.11532 - 0.04972\ P - 0.00470\ P^2$
$5.37941 < P \leq 7.13983$	$F12 = 0.05460 - 0.39421\ P + 0.05345\ P^2$
$7.13983 < P$	$F12 = 3.46726 - 0.67168\ P + 0.02538\ P^2$

ii) F22

$P \leq 5.67479$	$F22 = 0.21648\ P + 0.04124\ P^2$
$5.67479 < P \leq 7.12369$	$F22 = 4.32585 - 0.95156\ P + 0.11274\ P^2$
$7.12369 < P$	$F22 = 3.04962 - 1.66408\ P + 0.23791\ P^2$

iii) F52

$P \leq 4.84706$	$F52 = 0.01797 - 0.21348\ P - 0.01096\ P^2$
$4.84706 < P \leq 7.25805$	$F52 = 1.38431 - 0.61582\ P + 0.01389\ P^2$
$7.25805 < P$	$F52 = 1.71834 + 0.02564\ P - 0.08083\ P^2$

Low Pressure Tares due to Interference of Floating Leg #1 and Floating Leg #2

$P = \sqrt{Pa \times Pb}$ = characteristic pressure (psig)

i) F13

$p \leq 4.95776$	$F13 = 0$
$4.95776 < P \leq 7.05797$	$F13 = -8.91216 + 3.15307\ P - 0.27340\ P^2$
$7.05797 < P$	$F13 = -0.88253 + 0.11829\ P - 0.00461\ P^2$

ii) F23

$P \leq 4.14596$	$F23 = 0$
$4.14596 < P \leq 5.55160$	$F23 = 0.68968 - 0.16635\ P$
$5.55160 < P \leq 7.06837$	$F23 = 20.52929 - 7.31370\ P + 0.64372\ P^2$
$7.06837 < P$	$F23 = -5.08916 + 1.37559\ P - 0.07284\ P^2$

iii) F53

$P \leq 5.40104$	$F53 = 0$
$5.40104 < P \leq 7.12114$	$F53 = -7.08076 + 2.62302\ P - 0.24292\ P^2$
$7.12114 < P$	$F53 = 9.73929 - 2.38141\ P + 0.12815\ P^2$

High Pressure Tares

p = Pd = characteristics pressure in the high pressure air supply system (psig)
= test rig pressure measured near the entrance of the primary nozzle

a) before the heater was installed

$F14 = 0.0086633890 - 0.0096764591\ P + 0.0000593698\ P^2$

$F24 = 0.0111172866 - 0.0125054555\ P + 0.0000722089\ P^2$

$F54 = -0.0045751809 - 0.0065883921\ P + 0.0000651055\ P^2$

b) after the heater was installed

i) F14

$P \leq 63.5838$	$F14 = -0.015595 - 0.0039972\ P + 0.000064855\ P^2$
$63.5838 < P$	$F14 = -0.43874 + 0.011654\ P - 0.000076632\ P^2$

ii) F24

$P \leq 56.59$ $\quad F24 = -0.009093 - 0.0066227\ P + 0.00007366\ P^2$

$56.59 < P$ $\quad F24 = -0.3995 + 0.0086566\ P - 0.00007443\ P^2$

iii) $F54 = -0.066181 - 0.014812\ P$

Temperature Corrections of the High Pressure System

$P = Pd$ = characteristic pressure (psig)

$\Delta T = T_{op} - T_{\infty}$ (deg. F)

$Dfx = 0.0000111662\ P\ \Delta T$

$Dfy = (3.46581 - 0.0380987\ P)\ \Delta T\ /\ 1000$

Figure A-2 illustrates the sum of the thrust load cell readings (F01 + F02) compared to the sum of F10, F11, F12, F13, F20, F21, F22, and F23, when the entire low pressure air system was pressurized (no flow).

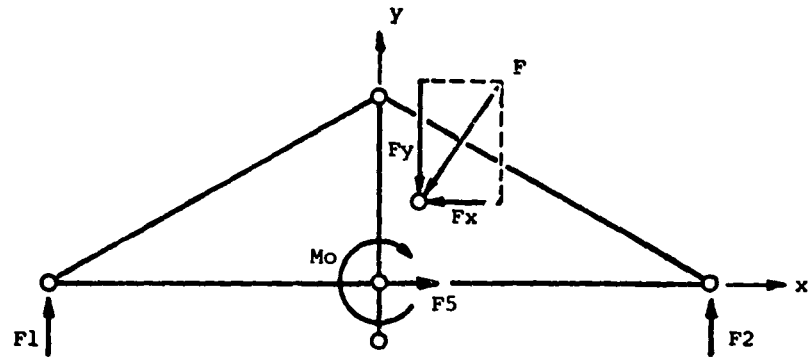

Figure A-1. Coordinate system for the FDRC static test rig

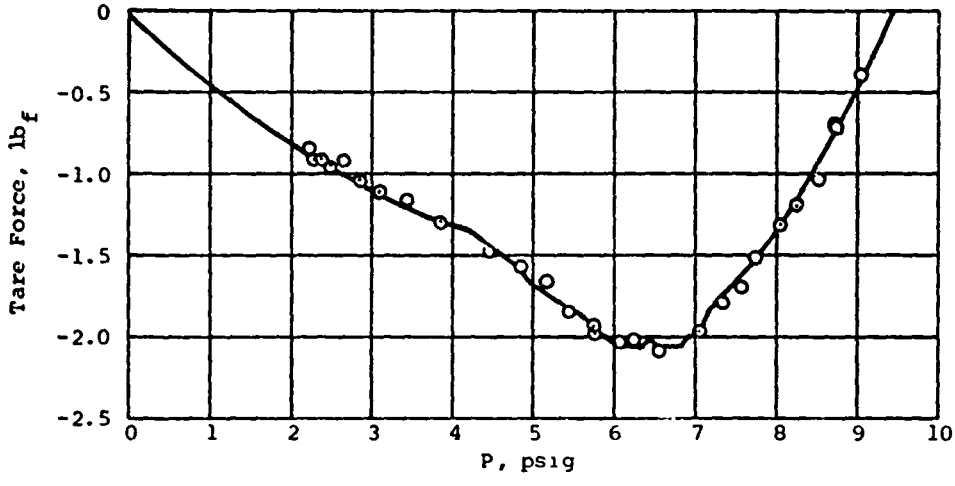

Figure A-2. Tares due to pressurization of the entire low pressure system

APPENDIX B

Mass Flow Measurement of the Low Pressure System

The FDRC static test rig has two sharp edge orifice flow meters on each low pressure air supply line (Figure 11) for mass flow rate measurements. The orifice diameter is 3.000", and the supply ducts are 5" pipes (5.047" I. D.). The installation of these two flow meters is not of the standard ASME type. Calibration procedures were discussed in "Data Reduction." Experimental measurements include downstream orifice pressure, differential pressure, and the total temperature of the flow. The discharge coefficient (C) was correlated to the uncorrected orifice Reynolds number (R = Reynolds number / discharge coefficient) using various empirical factors suggested in Reference 8. Unfortunately, corrections to this discharge coefficient were necessary for different ejector models under different test conditions. The examples of the correction factors shown in this Appendix were used for the data reduction of the test of the hot gas ejector shown on Figure 19.

Basic Relation

i) Leg #1

$$C = 0.44614 + 1.2373E\text{-}6\ R - 2.9837E\text{-}12\ R^2 + 2.2139E\text{-}18\ R^3$$

ii) Leg #2

$$C = 0.48335 + 8.2826E\text{-}7\ R - 1.9371E\text{-}12\ R^2 + 1.4026E\text{-}18\ R^3$$

Correction Factors

The mass flow rate of the secondary flow is the sum of the mass flow rate measured by each leg of the air supply system. However, corrections are necessary for various ejector models at different test conditions. Generally, the correction factor (Cf) can be obtained by correlating 1) correction factor (Cf) to the plenum pressure of the secondary flow (P), and 2) uncorrected Reynolds number (R) to the plenum pressure of the secondary flow (P), at different ejector outlet settings for different range of mass flow rates. Three sets of these relations (for outlet area ratios of approximately 0.8, 0.9, and 1.0) are provided for the following examples, which were used for the mass flow calculation of the secondary flow for the tests of the hot gas ejector shown on Figure 19. For a given value of the secondary plenum pressure (P - psig), the functional relation of Cf vs. R can be established by three sets of points, (R1, Cf1), (R2, Cf2), and (R3, Cf3). The correction factor (Cf) can be obtained by means of interpolation using the known value of R and the three point functional relationship. The overall discharge coefficient is (C x Cf).

a) Cold Primary Flow

i) R1 (outlet area ratio = 0.8)

$P \leq 5.9986$	$R1 =$	$111300 + 23458\ P$
$5.9986 < P \leq 7.2674$	$R1 =$	$513790 - 118040\ P + 12403\ P^2$
$7.2674 < P \leq 7.3540$	$R1 =$	$-425610 + 101360\ P$
$7.3540 < p$	$R1 =$	$-2049500 + 523890\ P - 27429\ P^2$

ii) R2 (outlet area ratio = 0.9)

$P \leq 6.0790$	$R2 =$	$124320 + 25820\ P$
$6.0790 < P \leq 7.2745$	$R2 =$	$594180 - 138250\ P + 14275\ P^2$
$7.2745 < P \leq 7.7832$	$R2 =$	$-495440 + 115380\ P$
$7.7832 < P$	$R2 =$	$-431770 + 160570\ P - 6857.1\ P^2$

iii) R3 (outlet area ratio = 1.0)

$P \leq 5.9702$	$R3 =$	$128150 + 29122\ P$
$5.9702 < P \leq 7.1690$	$R3 =$	$536220 - 117600\ P + 13127\ P^2$
$7.1690 < P \leq 7.6271$	$R3 =$	$-305640 + 93938\ P$
$7.6271 < P$	$R3 =$	$-454240 + 174200\ P - 7968.8\ P^2$

iv) Cf1 (outlet area ratio = 0.8)

$P \leq 6.2637$	$Cf1 =$	$0.82863 + 0.070071\ P - 0.0085332\ P^2$
$6.2637 < P \leq 7.9662$	$Cf1 =$	$-0.62267 + 0.55503\ P - 0.048966\ P^2$
$7.9662 < P$	$Cf1 =$	0.6914

v) Cf2 (outlet area ratio = 0.9)

$P \leq 6.3422$	$Cf2 =$	$0.84338 + 0.064105\ P - 0.0077224\ P^2$
$6.3422 < P \leq 7.8442$	$Cf2 =$	$-0.65221 + 0.56317\ P - 0.04923\ P^2$
$7.8442 < P$	$Cf2 =$	0.7362

vi) Cf3 (outlet area ratio = 1.0)

$P \leq 6.4553$	$Cf3 =$	$0.84958 + 0.061143\ P - 0.0083523\ P^2$
$6.4553 < P \leq 7.6985$	$Cf3 =$	$-0.53796 + 0.50831\ P - 0.044326\ P^2$
$7.6985 < P$	$Cf3 =$	0.7482

b) Hot Primary Flow

This set of data was a result of testing conducted to simulate the hot gas experiments, where the secondary plenum pressure was maintained at 3 psig between tests.

i) R1 (outlet area ratio = 0.8)

$P \leq 5.9047$	$R1 = 84177 + 28199\ P$
$5.9047 < P \leq 7.6010$	$R1 = 385900 - 79837\ P + 9642.7\ P^2$
$7.6010 < P \leq 8.2170$	$R1 = -8865200 + 2253100\ P - 137160\ P^2$
$8.2170 < P$	$R1 = 387600$

ii) R2 (outlet area ratio = 0.9)

$P \leq 6.0676$	$R2 = 94206 + 30816\ P$
$6.0676 < P \leq 7.0902$	$R2 = 578610 - 137290\ P + 14548\ P^2$
$7.0902 < P \leq 8.4804$	$R2 = -2200000 + 614730\ P - 36244\ P^2$
$8.4804 < P$	$R2 = 406590$

iii) R3 (outlet area ratio = 1.0)

$P \leq 5.5519$	$R3 = 103090 + 32942\ P$
$5.5519 < P \leq 7.1904$	$R3 = 387420 - 73437\ P + 9936.4\ P^2$
$7.1904 < P \leq 8.4040$	$R3 = -1469400 + 447830\ P - 26644\ P^2$
$8.4040 < P$	$R3 = 412370$

iv) Cf1 (outlet area ratio = 0.8)

$P \leq 5.7576$	$Cf1 = 1.0619 - 0.014116\ P - 0.0020148\ P^2$
$5.7576 < P \leq 7.9837$	$Cf1 = 0.31159 + 0.25462\ P - 0.026056\ P^2$
$7.9837 < P$	$Cf1 = 0.6836$

v) Cf2 (outlet area ratio = 0.9)

$P \leq 6.7192$	$Cf2 = 0.98226 + 0.024322\ P - 0.0063736\ P^2$
$6.7192 < P \leq 7.7869$	$Cf2 = 0.19332 + 0.28535\ P - 0.027747\ P^2$
$7.7869 < P$	$Cf2 = 0.73285$

vi) Cf3 (outlet area ratio = 1.0)

$P \leq 3.1552$	$Cf3 = 1.0167 - 0.012566\ P$
$3.1552 < P \leq 4.5991$	$Cf3 = 1.0859 - 0.034498\ P$
$4.5991 < P \leq 5.7783$	$Cf3 = 1.0407 - 0.02467\ P$
$5.7783 < P \leq 7.4182$	$Cf3 = 1.3659 - 0.08095\ P$
$7.4182 < P$	$Cf3 = 0.7654$

End of Document